Cell surface vimentin is involved in matrix stiffness-dependent infection of endothelial cells by *Listeria monocytogenes*

Effie E. Bastounis[1], Yi-Ting Yeh[2], and Julie A. Theriot[1,3,4]

[1] Department of Biochemistry, Stanford University School of Medicine, Stanford, California, USA

[2] Department of Bioengineering, University of California San Diego, La Jolla, California, USA

[3] Department of Microbiology and Immunology, Stanford University School of Medicine, Stanford, California, USA

[4] Howard Hughes Medical Institute, Stanford University School of Medicine, Stanford, California, USA

*To whom correspondence should be addressed: theriot@stanford.edu

Running title: Vimentin-mediated *Listeria monocytogenes* infection of endothelial cells

Keywords: *Listeria monocytogenes*, microvascular endothelial cells, matrix stiffness, polyacrylamide hydrogel, mechanotransduction, bacterial adhesion, focal adhesion kinase, cell surface vimentin

ABSTRACT

Vascular endothelial cells (VECs) line the inner lumen of vessels forming a protective barrier against spread of bacterial infection from the bloodstream into underlying tissue. VECs display remarkable phenotypic heterogeneity in part due to the different mechanical stimuli transmitted from their extracellular environment. Although VEC response to mechanical signals has been studied extensively, how bacterial uptake occurs in VECs residing on substrates of varying stiffness has not been explored. We use *Listeria monocytogenes*, a facultative intracellular bacterial pathogen, to determine the biophysical relationships between the stiffness of the matrix underlying VECs and bacterial infection. We report that adhesion of *L. monocytogenes* to human microvascular endothelial cells (HMEC-1), and therefore subsequent infection of the host cells, increases monotonically with increasing matrix stiffness, an effect that requires the activity of focal adhesion kinase (FAK). We identified cell surface vimentin as a candidate surface receptor mediating stiffness-dependent adhesion of *L. monocytogenes* to HMEC-1 and found that bacterial infection of these host cells is inhibited when surface vimentin is blocked with an antibody or pharmacologically, or when vimentin expression is knocked down. Although the interaction between the host cell receptor Met and the bacterial virulence factor InlB contributes to invasion of HMEC-1 by *L. monocytogenes*, this interaction does not affect initial adhesion of bacteria to the host cell surface and is not sensitive to substrate stiffness. Our results identify a novel pathway wherein increased extracellular matrix stiffness sensed by VECs leads to enhanced FAK activity that augments the amount of vimentin exposed at the surface of VECs, that in turn increases adhesion and uptake of *L. monocytogenes*.

INTRODUCTION

Vascular endothelial cells (VECs) line the inner lumen of blood vessels forming a physical barrier that tightly regulates the movement of vascular components from the bloodstream into underlying tissues. Despite the restrictive nature of the endothelium, certain bacterial pathogens can invade VECs and bypass the endothelial barrier to eventually infect surrounding tissues (1).

VECs throughout the body reside in highly variable environments that are rich and diverse in mechanical cues, such as extracellular matrix (ECM) stiffness, shear stresses due to blood flow and topography (2-5). VECs can both sense and adapt to the physical cues they experience which can vary in space (location within the vascular tree), in time (aging) and in pathophysiological conditions (e.g. arteriosclerosis) (6-10). For example, the local compliance of the basement membrane of VECs in the brain tissue is as soft as 1 kPa, while porcine aortas have been shown to have a stiffness of approximately 60-70 kPa (11-15). VECs express integrins, transmembrane receptors that allow attachment of the cells to their matrix through direct binding to ECM ligand proteins allowing them to probe features of their environment including its stiffness (16, 17). Integrin binding to the ECM leads to recruitment of additional proteins and to formation of focal adhesions that in turn relay information to the actin cytoskeleton and to various signaling molecules, modulating cellular adhesion, shape, contractility, gene expression and fate in general (18). Focal adhesion kinase (FAK) is a non-receptor tyrosine kinase that has been established as a key component of the signal transduction pathways triggered by integrins. The expression and/or activity of FAK is dependent on ECM rigidity, showing decreased expression and/or activation on softer matrices for certain cell types (19-22). Although it has long been known that ECM stiffness has a profound effect on VEC mechanics, motility, and interaction with circulating cells (6-8, 23, 24), little work has addressed mechanical effects on bacterial infection in these cells.

48 *Listeria monocytogenes* (Lm) is a ubiquitous food-borne facultative bacterial pathogen
49 that can move from the initial site of infection, the intestinal epithelium, to distant organs
50 protected by different types of vascular endothelium (25). When it crosses the microvasculature
51 of the brain it causes meningitis and encephalitis, while when it crosses the placenta it causes
52 spontaneous abortion (25, 26). Lm has a broad range of susceptible host animals, and uses
53 multiple pathogenic strategies to achieve infection of a wide variety of tissues within each host.
54 It can directly invade intestinal epithelial cells and hepatocytes, using bacterial surface proteins
55 belonging to the internalin family, such as InlA, InlB and InlF, which interact with host cell
56 receptors (27-30). Once internalized into a membrane-bound compartment, Lm expresses the
57 pore-forming toxin listeriolysin O (LLO), which promotes release of the bacterium into the
58 cytosol, where it replicates (31, 32). Lm then expresses the ActA protein, which triggers host cell
59 actin polymerization enabling intracellular bacterial propulsion and cell-to-cell spread (33-35).
60 Although epithelial infection by Lm and actin-based spread have been studied in depth,
61 relatively less is known about how this bacterium can access, directly infect and bypass the
62 endothelium, and the effect of the matrix stiffness of VECs on Lm infection has not been
63 explored (36, 37).

64 Bacterial adhesion to the surface of cells is typically the initial event in the pathogenesis
65 of infection and can occur through receptor-mediated interactions between the host cell and the
66 pathogen (38). Vimentin is generally an intracellular cytoskeletal protein that forms intermediate
67 filaments in many mesoderm-derived cells (39). Vimentin can also be localized on the surface of
68 cells for a variety of cell types, although the precise mechanism whereby vimentin is delivered to
69 the surface of cells is not yet fully understood (40-44). Recent studies have shown that various
70 bacteria as well as viruses use surface vimentin as attachment receptor to facilitate entry into
71 host cells (44-51). However, little is known about what modulates the amount of vimentin
72 exposed on the surface of cells and whether regulation of its surface presentation potentially

73 mediates bacterial uptake.

74 We examined Lm infection in endothelial cells derived from the microvasculature (human
75 microvascular endothelial cells, HMEC-1) cultured on matrices of varying stiffness to explore
76 how the stiffness of the local ECM of these cells affects their susceptibility to infection. We found
77 a two-fold increase in bacterial adhesion when cells reside on stiff as compared to soft matrices.
78 We also found that Tyr397 phosphorylation of FAK was higher for VECs residing on stiff
79 matrices, and furthermore that treatment of VECs with FAK inhibitors led to a dose-dependent
80 decrease in bacterial infection. When we searched for candidate VEC surface receptors
81 differentially modulated depending on FAK activity, we identified surface vimentin as a
82 candidate, and found that decreasing the amount of host surface vimentin leads to a
83 concomitant decrease in Lm infection. Taken together, our findings provide evidence that
84 environmental stiffness of VECs, a previously unappreciated factor, plays an important role in
85 regulating infection susceptibility to Lm through differential activity of FAK that in turn affects the
86 amount of surface vimentin.
87
88

RESULTS

Uptake of *Listeria monocytogenes* by HMEC-1 is more efficient when cells reside on stiff substrates.

Substrates on which vascular endothelial cells (VECs) are cultured *in vitro*, commonly glass or tissue culture (TC) polystyrene, are approximately six orders of magnitude stiffer than the natural ECM of human VECs (52, 53). To be able to recapitulate *in vivo* conditions and determine in a systematic way the effect of the VECs' matrix stiffness on the efficiency of *Listeria monocytogenes* (Lm) infection, we developed an assay based on manufacturing thin polyacrylamide hydrogels of varying stiffness ranging from 0.6 to 70 kPa on multi-well glass-bottom plates (54-56) (Suppl. Fig. 1A). To enable cell adhesion, hydrogels were surface-coated with collagen I, using a consistent density of collagen independent of hydrogel stiffness, as reported in previous studies (57-59). Human microvascular endothelial cells (HMEC-1) seeded for 24 h on the hydrogels formed monolayers with comparable densities regardless of substrate stiffness, similar to growth of these cells on TC polystyrene (Suppl. Fig. 1B)

In order to measure the efficiency of bacterial infection quantitatively, we infected HMEC-1 with a strain of Lm lacking expression of the ActA protein, thereby disabling actin-based bacterial cell-to-cell spread, so that changes in the number of infected cells could be directly attributable to the initial invasion event. This strain also expresses a fluorescent protein under a promoter that is activated several hours after exposure of the bacteria to the host cell cytosol (actAp::mTagRFP) (60), allowing reliable fluorescence-based detection only of bacteria that have successfully invaded the host cells. We determined the fraction of HMEC-1 infected with Lm in each well using flow cytometry (Fig. 1A-D). At a constant multiplicity of infection (MOI) and constant host cell density, we found a monotonic increase in the number of VECs infected by Lm with increasing hydrogel stiffness that was highly reproducible among biological replicates (Fig. 1E-F). The overall efficiency of infection on the stiffest hydrogel substrates tested, 70 kPa, was comparable to the efficiency of infection for the same cells grown on TC

115 polystyrene, suggesting that above a certain level of stiffness the infection efficiency does not
116 change (Fig. 1F). Compared to this maximum level of infection for HMEC-1 cultured on the
117 stiffest substrates, infection efficiency on the softest substrates decreased about two-fold (Fig.
118 1E-F).
119
120 **HMEC-1 on soft hydrogels show decreased FAK activity and decreased FAK activity**
121 **leads to less efficient Lm infection.**
122 Focal adhesion kinase (FAK) has been established as a key component of the signal
123 transduction pathways triggered by integrins binding to the ECM, and for some cell types FAK
124 expression and/or phosphorylation on residue Y397 have been shown to depend on mechanical
125 cues sensed by cells, such as shear stresses imposed by fluid flow and/or ECM rigidity (19-22,
126 61). We therefore sought to determine whether FAK expression or activity could be modulated
127 depending on the substrate stiffness where HMEC-1 reside. To that end, HMEC-1 were grown
128 on soft 3 kPa hydrogels, stiff 70 kPa hydrogels and TC polystyrene substrates treated with
129 vehicle control or PF573228 FAK inhibitor. Cells were then harvested and total amounts of FAK
130 as well as pY397-FAK were determined using Western blot analysis. We found that increasing
131 the stiffness of the underlying substrate from 3 kPa to 70 kPa resulted in increasing levels of
132 pY397-FAK, but the levels of total FAK remained largely unchanged (Fig. 2A-C). In addition, the
133 levels of pFAK-Y397 were similar for cells residing on stiff 70 kPa hydrogels as compared to TC
134 polystyrene substrates (Fig. 2A-C). Treating cells residing on polystyrene with the specific FAK
135 inhibitor PF573228 led to a significant decrease of pY397-FAK while total FAK levels remained
136 unchanged as compared to controls (Fig. 2A-C). Our results suggest that FAK phosphorylation
137 at Y397 is modulated by the stiffness of the substrate on which HMEC-1 reside and therefore by
138 different levels of cell–ECM interaction-induced focal adhesion signaling.
139 To address whether reduced Lm uptake as observed for HMEC-1 residing on soft
140 matrices can be attributed at least in part to reduced FAK activity, we treated HMEC-1 residing

141 on polystyrene substrates with FAK inhibitors FAK-14 or PF573228 for one hour prior to
142 infection. We then measured the efficiency of infection with Lm as described above, and found
143 that both FAK inhibitors caused a similar dose-dependent inhibition of Lm infection (Figs. 2D).
144 Taken together these results are consistent with the hypothesis that decreased bacterial
145 infection of HMEC-1 residing on highly compliant soft matrices may be in part due to decreased
146 FAK activity.
147
148 **Adhesion but not invasion efficiency is increased when Lm infect HMEC-1 residing on**
149 **stiff substrates.**
150 Decreased infection efficiency of Lm in HMEC-1 residing on soft matrices or treated with
151 FAK inhibitors could be due to quantitative changes at several different steps in the infection
152 process, for example decreased bacterial adhesion onto HMEC-1, or decreased invasion of the
153 adhering bacteria into the HMEC-1, or a combination of both. To help identify the exact step in
154 infection that is sensitive to substrate stiffness, we used a constitutively GFP-expressing strain
155 of Lm to infect HMEC-1 residing on either soft 3 kPa hydrogels or stiff 70 kPa hydrogels, and
156 treated with vehicle control or PF573228. Samples were fixed shortly after infection and bacteria
157 that were attached to the cell surface but not yet internalized were specifically labeled with
158 antibodies under non-permeabilizing conditions. This inside/outside labeling method allows us
159 to distinguish between bacteria that are adhered but not internalized (GFP-positive and labeled
160 with the antibody) and those that are fully internalized by the HMEC-1 (GFP-positive but not
161 labeled with the antibody). We found that both the total number of bacteria per host cell and the
162 number of internalized bacteria per cell are significantly increased when HMEC-1 reside on stiff
163 70 kPa hydrogels as compared to soft 3 kPa hydrogels (Fig. 3A-B). However, importantly, the
164 invasion efficiency (ratio of internalized bacteria to total bacteria) did not differ between HMEC-1
165 residing on stiff as compared to soft matrices, suggesting that it is specifically the adhesion of
166 bacteria to the surface of host cells that is increased when the matrix stiffness is elevated and

167 which leads to increased Lm infection efficiency for cells residing on stiffer matrices (Fig. 3C).
168 Interestingly, we found a decrease in both Lm adhesion and invasion efficiency irrespective of
169 hydrogel stiffness for the cells treated with the FAK inhibitor (Fig. 3), suggesting that FAK
170 activity levels modulate both adhesion and invasion efficiency of Lm in HMEC-1, while substrate
171 stiffness affects adhesion only.
172
173 **InlB contributes to Lm infection of HMEC-1 but is not modulated by substrate stiffness**.
174 Our data indicate that lower FAK activity as it occurs when HMEC-1 are seeded on
175 softer hydrogels leads to decreased Lm adhesion onto the surface of HMEC-1. This finding led
176 us to hypothesize that a receptor at the surface of cells could be differentially regulated
177 depending on substrate stiffness, leading to decreased bacterial adhesion. To examine whether
178 any of the Lm internalins known to play a role in adhesion or invasion of other cell types,
179 including VECs, is implicated in infection of HMEC-1 and responsible for the matrix stiffness
180 dependent susceptibility to infection, we infected HMEC-1 with mutant strains deficient in each
181 of the internalin-encoding genes *inlA*, *inlB* or *inlF* (Fig. 4A and Table S1). We found a two-fold
182 decrease in bacterial infection when InlB was not present, suggesting that InlB is one of possibly
183 multiple bacterial factors that contribute to Lm infection of HMEC-1. In contrast to the effect of
184 the deletion in the *inlB* gene, deletion of *inlF* had no effect in bacterial infection of HMEC-1.
185 Deletion of *inlA* resulted in very modest but reproducible reduction in infection as reported
186 previously for human brain microvascular endothelial cells infected with Lm (62).
187 The importance of InlB for initial invasion of Lm into HMEC-1 was further confirmed by
188 infecting HMEC-1 with a different strain that had deletions in both *inlB* and *actA* so that bacteria
189 could not spread from cell to cell. Consistent with our previous findings, we observed a two-fold
190 decrease in bacterial uptake for a series of different multiplicities of infection (MOI) when *inlB*
191 was knocked out (Fig. 4B). Importantly, bacteria carrying a deletion of *inlB* still exhibited a
192 strong monotonic dependence of infection efficiency on substrate stiffness (Fig. 4C and Suppl.

193 Fig. 2A). This finding indicates that, while InlB contributes to some step in the infection of
194 HMEC-1 by Lm, it is not governing the step that is sensitive to substrate stiffness.
195 We confirmed this conclusion using three different lines of experimentation. First, we
196 directly assessed the effect of *inlB* deletion on bacterial adhesion and invasion of HMEC-1 using
197 inside/outside labeling as described above. We found that the total number of bacteria
198 associated with HMEC-1 cells was the same for wild-type bacteria as compared to an isogenic
199 *ΔinlB* strain (Fig. 4D), that is, adhesion to the host cell surface is indeed unchanged. However,
200 the number of internalized bacteria per cell and therefore the overall invasion efficiency was
201 significantly decreased for the *ΔinlB* strain (Fig. 4E-F). Second, we examined the effect of
202 inhibiting the host cell binding partner for InlB, the receptor tyrosine kinase Met (also known as
203 the hepatocyte growth factor receptor), on bacterial invasion. We confirmed that HMEC-1
204 express Met (Suppl. Fig. 1C), and then treated the cells with varying concentrations of the highly
205 selective Met inhibitor SGX-523 prior to infection (63). We found that only uptake of the control
206 Δ*actA* strain of Lm decreased with increasing concentration of SGX-523, while uptake of the
207 isogenic Δ*actA*/Δ*inlB* Lm did not change substantially as a function of SGX-523 concentration
208 (Fig. 4G). These results confirm that InlB contributes to Lm invasion into HMEC-1 by interacting
209 with host Met as has been shown for other cell types (27, 28). However, Lm invasion into
210 HMEC-1 treated with SGX-523 still retains a strong dependence on substrate stiffness (Fig. 4H
211 and Suppl. Fig. 2B). Third, we found that infection of HMEC-1 with the Δ*actA*/Δ*inlB* strain of Lm
212 is still highly sensitive to inhibition of FAK with PF573228, showing a dose-response curve that
213 parallels that of the control Δ*actA* strain (Fig. 4I).
214 So far we can conclude that substrate stiffness affects the adhesion of Lm to the surface
215 of HMEC-1 such that bacterial adhesion to host cells residing on soft substrates is about two-
216 fold less than to host cells residing on stiff substrates. The well-characterized InlB-Met
217 interaction contributes to invasion of adherent bacteria into HMEC-1, and is responsible for

218 about half of the invasion efficiency for Lm infecting these cells, however this interaction does
219 not govern bacterial adhesion per se and is not sensitive to substrate stiffness. We therefore
220 sought to identify alternative possible host cell receptors for adhesion of Lm to the surface of
221 HMEC-1 that might be responsible for the stiffness-dependent effects we consistently observe.
222
223 **Inhibiting FAK activity leads to reduced amount of cell surface vimentin for HMEC-1.**
224 Since the decreased FAK activity associated with growth of HMEC-1 on softer hydrogels
225 leads to decreased Lm adhesion onto the surface of host cells, we attempted to identify
226 candidate host surface receptors whose amount is modulated by FAK activity and which
227 mediate bacterial adhesion. Since manufacturing soft and stiff PA hydrogels with large
228 dimensions is both technically challenging and costly, we instead grew cells on large TC
229 polystyrene plates and treated them with vehicle control or the FAK inhibitor PF573228. We
230 then biotinylated the cell surface-exposed proteins using membrane-impermeable EZ-Link
231 Sulfo-NHS-SS-Biotin and isolated them by affinity chromatography with streptavidin-agarose
232 beads (64, 65). Isolated surface proteins were then run in 2D-PAGE gels to allow separation of
233 proteins according to both their isoelectric points and their molecular weight (66). Gels were
234 silver stained and comparison between gels was performed by marking the spots that differed in
235 intensity (Fig. 5A-B). We found a spot at approximately 55 kDa consistently differing in two
236 independent experiments between the control sample and the sample treated with the FAK
237 inhibitor PF573228 (see circles in Fig. 5A-B). In a third replicate experiment of surface protein
238 isolation, 2D-PAGE gels were Coomassie stained and that specific 55 kDa spot that differed as
239 a function of FAK inhibitor treatment was excised and further analyzed by nanoliquid
240 chromatography tandem mass spectrometry (nanoLC-MS/MS). We identified this spot as the
241 protein vimentin (accession number: gi|340219, Mascot identification score: 788, number of
242 identified peptides: 87, mass: 53752, isoelectric point: 5.05, sequence coverage: 61%).
243 Vimentin is a major component of the cytoskeleton forming intermediate filaments, but exists

244 also in soluble form and has been previously found to localize at the cell surface for a wide
245 variety of cells including VECs (41, 47, 50, 51, 67).
246 Given the high validity of identification, we sought to confirm whether vimentin is
247 expressed at the surface of HMEC-1 by performing immunostaining of non-permeabilized
248 HMEC-1 seeded on collagen I-coated glass substrates followed by epifluorescence imaging
249 (Fig. 6). For negative controls, cells were incubated with secondary antibody alone. The anti-
250 vimentin H-84 antibody stained the vimentin intermediate filaments of permeabilized cells very
251 well (Fig. 6A-C). Non-permeabilized cells showed surface staining of vimentin near cell-cell
252 junctions, while staining was less prominent for cells treated with the FAK inhibitor PF537228
253 and very low background staining was observed for cells incubated with secondary antibody
254 alone (Fig. 6D-F). This localization confirmed that cell surface vimentin could be a plausible
255 candidate responsible for adhesion of Lm to HMEC-1.
256
257 **HMEC-1 surface vimentin contributes to Lm uptake.**
258 To determine whether surface vimentin specifically contributes to Lm adhesion and
259 thereby infection of HMEC-1, we used three independent methods to decrease the availability of
260 cell surface vimentin for bacterial adhesion. First, we pretreated HMEC-1 with varying
261 concentrations of H-84 anti-vimentin antibody prior to infection with Lm, and found a dose-
262 dependent decrease in infection efficiency (Fig. 7A). We found a maximum two-fold decrease in
263 Lm infection when incubating cells with 80 μg/ml anti-vimentin antibody, while increasing further
264 the concentration of the antibody did not lead to further decrease in Lm uptake (Suppl. Fig. 3A).
265 Second, HMEC-1 were transfected with commercial non-targeting control siRNA (siNT)
266 or siRNA targeting vimentin (siVIM) and total vimentin expression was found to be five-fold
267 reduced for the vimentin knockdown cells as compared to controls through RT-PCR (Suppl. Fig.
268 4E and Tables S2-S3). We found a significant decrease (about 30%) in Lm infection efficiency

269 for the vimentin knockdown cells as compared to control cells, while confirming that cell
270 confluency under both conditions was similar (Fig. 7B; Suppl. Fig. 3A-D).
271 Third, we treated HMEC-1 cells with varying concentrations of withaferin, a natural
272 product known to bind the soluble form of vimentin (68-70). We found a dose-dependent
273 decrease in infection efficiency for Lm in withaferin-treated cells, again finding a maximum two-
274 fold decrease when cells were treated with 5-10 μM of withaferin prior to infection (Fig. 7C).
275 Higher concentrations of withaferin disrupted HMEC-1 cell-substrate adhesion. Overall these
276 results are consistent with the hypothesis that cell surface vimentin is responsible for about half
277 of the amount of adhesion of Lm to the HMEC-1 surface, and that vimentin presentation on the
278 cell surface is sensitive to substrate stiffness.
279 To examine any possible interaction between the contribution of vimentin-based
280 adhesion and the contribution of InlB/Met-based invasion of Lm infecting HMEC-1, we
281 pretreated HMEC-1 with withaferin or vehicle control and then infected with either Δ*actA* or
282 Δ*actA/* Δ*inlB* Lm over a range of multiplicities of infection (MOI). Consistent with our results
283 described above, we found a two-fold decrease in Lm uptake when cells were pretreated with
284 withaferin and infected with Δ*actA* Lm or when cells were not treated with withaferin but were
285 infected with Δ*actA/* Δ*inlB* Lm (Fig. 7D). When cells were both pretreated with withaferin and
286 infected with Δ*actA/* Δ*inlB* Lm, infection was decreased four-fold relative to control (Fig. 7D), i.e.
287 InlB/Met and vimentin contribute independently to infection efficiency. However, under all
288 conditions there was still residual infection, suggesting that Lm uses additional strategies to
289 achieve uptake by HMEC-1, other than interactions with surface vimentin for bacterial adhesion
290 and with Met for increased bacterial internalization.
291
292 **Uptake of *Listeria innocua* but not carboxylated latex beads by HMEC-1 depends on cell**
293 **surface vimentin.**

294 Our results demonstrate that the vimentin-dependent adhesion of Lm to HMEC-1 is
295 sensitive to substrate stiffness and is not mediated by the bacterial internalins InlA, InlB, or InlF.
296 In order to gain insight into whether vimentin-based bacterial adhesion is a result of a non-
297 specific stickiness or a specific host-bacterium interaction, we measured the influence of cell
298 surface vimentin on adhesion of other bacteria and of non-biological particles. *Listeria innocua*
299 (Li) is a bacterium closely related to Lm that is considered non-pathogenic in that it lacks the
300 putative internalin family members and other virulence factors that Lm carries (71). When we
301 infected HMEC-1 with comparable loads of Lm and Li, we found that adhesion of both bacteria
302 is comparable (Fig. 8A). We also found that treating HMEC-1 with FAK inhibitor PF537228 or
303 blocking HMEC-1 with anti-vimentin antibody H-84 reduces adhesion of both Lm and Li onto
304 HMEC-1 by similar amounts (Fig. 8A). Next, to examine whether a bacterial factor common in
305 Lm and Li could responsible for surface vimentin mediated adhesion, we blocked HMEC-1 with
306 anti-vimentin antibody and exposed cells to 2 μm carboxylated latex beads, which are efficiently
307 taken up by VECs. We found that uptake of beads did not vary with antibody concentration and
308 was identical to uptake of cells treated with isotype control (Fig. 8B). Our results suggest that
309 cell surface vimentin is a common receptor for both Lm and Li in the context of adhesion to
310 HMEC-1, but uptake of nonbiological particles such as carboxylated latex beads does not
311 depend on surface vimentin.
312
313

314 **DISCUSSION**

315 **Bacterial infection of VECs depends on the stiffness of the matrix on which cells reside.**

316 Our data demonstrate that susceptibility of HMEC-1 cells to Lm infection depends on the
317 stiffness of the matrix on which cells reside. Mechanosensitive cells, such as VECs, can "feel" a
318 variety of physical cues such as fluid shear stresses, cyclic strains, matrix stiffness and respond
319 to them by altering their morphology, gene expression and function (72). Interestingly, many
320 signaling pathways involved in mechanotransduction are common irrespective of the exact
321 mechanical stimulus (73, 74). For instance, exposure of VECs to laminar shear stress leads to
322 recruitment of FAK at focal adhesions and to an increase in the phosphorylation at Y397 (73).
323 Consistent with FAK activity being sensitive to mechanical stimuli, we found that FAK activity is
324 increased when cells reside on stiffer PA hydrogels. Concurrently, we observe a decrease in Lm
325 uptake when FAK activity is reduced or inhibited. It is possible that enhanced FAK activity for
326 VECs exposed to high shear stresses, might also lead to increased Lm uptake, but this still
327 remains to be investigated (73). Our findings also suggest that the stiffness of the environment
328 where cells reside is an additional variable worth exploring since it affects cellular behavior and
329 susceptibility to bacterial infection and it is not taken into account in traditional studies of
330 bacterial infection of host cells that are commonly performed on non-physiological glass or
331 polystyrene surfaces. We speculate that additional mechanical cues sensed by VECs might also
332 affect susceptibility of cells to infection. Therefore, the development of organotypic models for
333 studying bacterial infection, that take into account the *in vivo* mechanical cues sensed by cells is
334 pertinent and will aid our emerging understanding of the biomechanics of host-bacteria
335 interactions as well as the design of more effective therapeutic interventions that take into
336 consideration the local cellular mechanical micro-environment.

337

338 **Surface vimentin is a receptor for Listeria infection of VECs**.

339 We found that lower FAK activity as occurs when HMEC-1 are seeded on softer
340 hydrogels leads to decreased Lm and Li adhesion onto the surface of HMEC-1 and that is
341 attributable to lower levels of cell surface vimentin. The role of cell surface vimentin as an
342 attachment receptor facilitating bacterial or viral entry has been previously documented for other
343 pathogens (44-51). VEC surface vimentin in particular has been shown to be the receptor for
344 attachment of *E. coli* K1 and multiple viruses (47, 49, 51, 75, 76). We speculate that matrix
345 stiffness of VECs might possibly also affect uptake of the above viruses and bacteria, since the
346 amount of surface vimentin is reduced when FAK activity is decreased as in the case of cells
347 residing on highly compliant matrices.
348 Bacterial adhesion to the surface of cells is commonly required as a precursor to
349 invasion (77, 78). Our finding that both Lm and Li adhesion is reduced when HMEC-1 are
350 blocked with anti-vimentin antibodies suggests that the possible bacterial binding partner of
351 vimentin might be expressed in both bacterial species. Surface vimentin has been shown to
352 possess lectin-like activity binding N-acetylglucosamine (GlcNAc), a sugar that is also
353 commonly found as a component of bacterial cell envelopes (79, 80). Specifically, GlcNAc is
354 found decorating the wall teichoic acids of Lm serotype 1/2a strains, such as the 10403S strain
355 used in this study (81). That implies that bacterial carbohydrate-binding to host cell surface
356 vimentin might also be a plausible specific interaction.
357
358 **Lm uses multiple pathogenic strategies to infect VECs, some of which are independent**
359 **of ECM stiffness.**
360 We identified that the Lm virulence factor InlB interacts with HMEC-1 receptor Met and
361 that Lm uptake is decreased by two-fold when Met is inhibited, however this interaction is not
362 sensitive to matrix stiffness. When we infected HMEC-1 with Δ*actA*/Δ*inlB* Lm after treating host
363 cells with withaferin that binds to soluble vimentin, we found a four-fold decrease in infection
364 relative to controls, indicating that the vimentin-dependent and InlB-dependent pathways

365 contribute to infection independently of one another; however, even when both pathways were
366 blocked there was still residual Lm infection. This residual Lm infection suggests that there are
367 additional InlB-independent and vimentin-independent mechanisms that Lm leverage to infect
368 HMEC-1.

369 Increased Lm adhesion onto HMEC-1 residing on stiff matrices could be attributed to
370 multiple factors. In this work we investigated the possibility of a receptor at the surface of host
371 cells being differentially regulated when FAK activity is increased, as in stiff matrices, and
372 identified cell surface vimentin as a well-supported candidate receptor. However, it is also
373 possible that additional factors might also lead to the decreased adhesion of Lm onto HMEC-1
374 residing on softer matrices. It is plausible that the cell surface glycans of HMEC-1 might be
375 differentially regulated depending on the stiffness of the environment. For example previous
376 studies have suggested both a positive correlation between FAK activity and the heparan
377 sulfate portion of the glycocalyx (82, 83) and between the heparan sulfate portion of the
378 glycocalyx and Lm adhesion onto enterocytes (84). Another possibility could be the differential
379 regulation of biophysical or mechanical properties of the host cells depending on matrix stiffness
380 (e.g. cell cortical stiffness, surface roughness, membrane tension). For instance, studies on
381 adhesion of bacteria onto hydrogel surfaces have shown that adherence is increased on stiffer
382 hydrogels (85), suggesting that if cells become stiffer on stiffer hydrogels, cellular stiffness alone
383 could lead to increased bacterial adhesion (22, 86).

384

385 **VEC origin and physical cues might explain discrepancy between previous studies on**
386 **VEC infection by Lm.**

387 The endothelial lining of blood vessels displays remarkable spatiotemporal heterogeneity
388 and the basis of these morphological and functional differences are still unclear (87-89). It is
389 well documented that mechanical and chemical cues relayed to VECs by their environment can
390 alter both function and gene expression of VECs found at different tissues (72, 90). However,

391 even when VECs from different origins are placed *in vitro* in the same biochemical and
392 mechanical environment, they can still exhibit unique characteristics and behaviors that are
393 intrinsic to the cells themselves and are not determined by differential culture or environmental
394 conditions (5, 91-93). For example, the response of human umbilical cord endothelial cells
395 (HUVEC) to changes in curvature or shear stress is completely distinct as compared to that of
396 human brain microvascular endothelial cells (HBMEC) (91). In accordance with the differences
397 these two cell types exhibit in response to geometrical constraints or mechanical stimuli, studies
398 have also shown differences with respect to Lm infection. Past studies suggest that HBMEC
399 infection by Lm depends on InlB (62), while HUVEC uptake of Lm appears to be independent of
400 both the internalins InlA and InlB (94, 95). These studies are not necessarily conflicting but
401 suggest that bacterial infection of VECs depends upon both the environment and the particular
402 origin of VECs and therefore conclusions should refer to the exact cell type and not to
403 endothelial cells in general. Since many pathological processes occur at the microvascular level
404 of organs (i.e. Lm infection of the brain microvasculature), we chose in this study to use HMEC-
405 1 as our model for VECs. However, extrapolation from results obtained for HMEC-1 infection by
406 Lm to other VECs should be performed with caution.
407 In conclusion, our results provide the first strong evidence that the local mechanical
408 environment and in particular the matrix stiffness of VECs regulates susceptibility of VECs to Lm
409 infection. The novel mechanosensitive pathway we identified suggests that increased ECM
410 stiffness sensed by VECs leads to enhanced FAK activity that augments the amount of vimentin
411 exposed at the surface of VECs. Increased amount of surface vimentin in turn increases Lm
412 adhesion and subsequent uptake by VECs. Our studies on the effect of ECM stiffness in
413 bacterial uptake of VECs can have other significant implications, since they provide an example
414 of how mechanotransduction can be exploited in biology and medicine facilitating the
415 development of therapeutic interventions against bacterial infections and other diseases.
416

417 **MATERIALS AND METHODS**

418 **Fabrication of thin two-layered polyacrylamide (PA) hydrogels on 24-well glass-bottom**
419 **dishes**

420 PA hydrogel fabrication was done as previously described with a few modifications for
421 the specific experiments (56, 96-98). 24-well glass bottom plates (MatTek, P24G-1.5-13-F) were
422 incubated for 1 h with 500 µl of 2 M NaOH. Wells were rinsed with distilled water, and 500 µl of
423 2% 3-Aminopropyltriethoxysilane (Sigma, 919-30-2) in 95% ethanol were added to each well for
424 5 min. Wells were rinsed again with water and 500 µl of 0.5% gluteraldehyde was added in each
425 well for 30 min. Wells were rinsed with water and dried at 60°C. To prepare hydrogels of varying
426 stiffness, mixtures containing 3–10% acrylamide (Sigma, A4058) and 0.06–0.6% bis-acrylamide
427 (Fisher, BP1404-250) were prepared. Specifically, 0.6 kPa hydrogels contained 3% acrylamide
428 and 0.06% bis-acrylamide, 3 kPa hydrogels contained 5% acrylamide and 0.1% bis-acrylamide,
429 20 kPa hydrogels contained 8% acrylamide and 0.26% bis-acrylamide, and 70 kPa hydrogels
430 contained 10% acrylamide and 0.6% bis-acrylamide. For each stiffness, two mixtures were
431 prepared the second of which contained 0.03% 0.1 µm diameter fluorescent beads (Invitrogen,
432 F8803). Mixtures were then degassed for 15 min to remove oxygen, which inhibits acrylamide
433 polymerization.

434 First, 0.06% APS and 0.43% TEMED were added to the solutions containing no beads
435 to initiate polymerization and then 3.6 µl of the mixture was added at the center of each well,
436 capped with 12 mm untreated circular glass coverslips and allowed to polymerize for 20 min.
437 The coverslips were then lifted with a syringe needle with a small hook at its tip and then 2.4 µl
438 of the mixture containing tracer beads was added, sandwiched again with a 12 mm untreated
439 circular glass coverslip, gently pressed downwards by means of forceps, and allowed to
440 polymerize for 20 min. 50 mM HEPES pH 7.5 was added in the wells, and coverslips were
441 removed using the syringe needle and forceps. PA hydrogels were UV-sterilized for 1 h.
442 Hydrogels were then activated by adding 200 µl 0.5% w/v heterobifunctional crosslinker Sulfo-

443 SANPAH (ProteoChem, c1111) in 1% DMSO and 50 mM HEPES pH 7.5 on the upper surface
444 of the hydrogels and exposing to UV light for 10 min. After activation, the hydrogels were
445 washed with 50 mM HEPES pH 7.5 to remove excess crosslinker and were coated with 200 µl
446 of 0.25 mg/ml rat tail collagen I (Sigma-Aldrich, C3867) in 50 mM HEPES overnight at room
447 temperature. Prior to seeding cells, hydrogels were incubated with cell media to allow
448 equilibration for 30 min.
449
450 **HMEC-1 culture and infection with *Listeria monocytogenes* (Lm)**
451 Human microvascular endothelial cells (HMEC-1, generous gift from Welch lab, UC
452 Berkeley) were maintained in MCDB 131 medium (Fisher Sci Co, 10372-019) supplemented
453 with 10% FBS (GemBio, 900-108), 10 ng/mL epidermal growth factor (Sigma, E9644), 1 µg/mL
454 hydrocortisone (Sigma, H0888), and 2mM L-glutamine (Sigma, 56-85-9).
455 HMEC-1 were infected as previously described with the following modifications (94).
456 The day prior to infection, host cells were seeded at a density of $4x10^5$ cells/well for cells
457 residing on wells of 24-well plates or at a density of $1x10^5$ cells/well for cells residing on wells of
458 48-well plates, and grown for 24 h. Lm liquid cultures were started from a plate colony, and
459 grown overnight, shaking, at 30°C in Brain Heart Infusion (BHI) media (BD, 211059)
460 supplemented with 200 µg/mL streptomycin and 7.5 µg/mL chloramphenicol. The day of the
461 infection, the O.D.600 of the overnight cultures was measured and diluted to 0.1. Samples were
462 incubated for 2 h shaking, in the dark at 30°C in BHI media supplemented with 200 µg/mL
463 streptomycin and 7.5 µg/mL chloramphenicol to allow the O.D. 600 to reach 0.2-0.3 and let
464 bacteria enter the logarithmic growth phase. Bacteria were then washed 3 times with PBS to
465 remove any soluble factors and infections were performed in normal growth media (99).
466 To synchronize invasion, Lm diluted in normal growth media were added on the HMEC-1
467 cells and samples were spun for 10 min at 200 x g prior to incubation. After 30 min of incubation
468 at 37 degrees, samples were washed 4 times in PBS and after an additional 30 min, media was

469 replaced with media supplemented with 20 µg/mL gentamicin. Multiplicity of infection (MOI) was
470 determined by plating bacteria at different dilutions, on BHI agar plates with 200 µg/mL
471 streptomycin and 7.5 µg/mL chloramphenicol and measuring the number of colonies formed 2
472 days post-infection. A similar approach was followed when HMEC-1 were infected with *Listeria*
473 *innocua* (Li), except that BHI plates with no antibiotics were used. All bacterial strains used in
474 these studied are indicated in Table S1.
475 Analysis of infection via flow cytometry was performed at 7-8 h after exposure, unless
476 otherwise stated. For drug exposure experiments, unless otherwise indicated, media was
477 removed from the cells and replaced with media containing either the drug or vehicle control 1 h
478 prior to infection or 30 min prior to infection for the case of withaferin. Cells were cultured in the
479 drug-containing media for 1 h after infection. 1 h post-infection cells were washed four times and
480 drug-free gentamicin-containing media was added to the cells.
481
482 **Antibodies and reagents**
483 Hoechst (Thermofisher, D1306) was dissolved at 1 mg/mL in dimethyl formamide
484 (DMSO) and used at 1:1000. Drugs were dissolved in DMSO (Sigma, D2650) at the stock
485 concentrations indicated: 10 mM FAK inhibitor-14 (FAK-14) (Tocris Bioscience, 3414), 100 mM
486 PF573228 (Tocris Bioscience, 3239), 20 mM SGX 523 (Tocris Bioscience *5356*), 42 mM
487 withaferin (Sigma-Aldrich, W4394). Primary antibody used for staining of extracellular Lm was
488 rabbit polyclonal anti-*Listeria* genus specific antibody (ABCAM, ab35132). Primary antibody
489 used for staining Li was goat polyclonal BacTrace anti-*Listeria* genus specific antibody
490 (SeraCare Life Sciences Inc., 01-90-90). For incubation of cells with vimentin antibodies prior to
491 infection or immunostaining of surface vimentin, rabbit polyclonal H-84 vimentin antibody (Santa
492 Cruz Biotechnologies, sc-5565) was used. For isotype controls, cells were incubated with rabbit
493 IgG (Sigma, I5006). For western blotting the following antibodies were used: rabbit polyclonal
494 phospho-FAK Tyr397 (ThermoFisher, 44-624G), mouse monoclonal anti-FAK (EMD Millipore,

495 05-182), rabbit monoclonal anti-Met (cMet) antibody (Abcam, ab51067), anti-GAPDH antibody
496 (Cell signaling, 140C10).
497
498 **Flow cytometry of HMEC-1 cells infected with Lm**
499 7-8 h post-infection, infected HMEC-1 cells were detached from the substrate by
500 incubating them for 10 minutes with a mixture of 200 µl of 0.25% trypsin-EDTA and 0.05%
501 collagenase (Sigma, C0130). Solutions in each well were pipetted up and down 6 times to
502 ensure single cell suspensions, and 200 µl of complete media was added to inactivate trypsin in
503 each well. Solutions were transferred into 5 ml polystyrene tubes with a 35 µm cell strainer cap
504 (Falcon, 352235) and then samples were immediately analyzed by flow cytometry on the
505 Scanford FACScan analyzer (Custom Stanford and Cytek upgraded FACScan). 10,000-20,000
506 cells were analyzed per each replicate.
507
508 **Immunostaining of extracellular adherent bacteria**
509 HMEC-1 cells residing on either PA hydrogel substrates or glass collagen I-coated
510 coverslips were infected as described above with a Lm strain that constitutively expresses GFP.
511 20 min post-infection, 1 µg/ml Hoechst (Thermofisher, D1306) was added in each well to stain
512 the cells' nuclei. 30 min post-infection cells were washed 4 times in PBS and fixed with a non-
513 permeabilizing fixative for differential immunostaining for 20 min at room temperature (100).
514 Fixative contained 0.32 M sucrose, 10mM MES pH 6.1, 138 mM KCl, 3 mM $MgCl_2$, 2 mM EGTA
515 and 4% formaldehyde EM grade. Following a wash with PBS, samples were blocked for 30
516 minutes with 5% BSA in PBS and then incubated with anti-Lm primary antibody (Abcam
517 ab35132) diluted 1:100 in PBS containing 2% BSA for 1 h. Samples were washed in PBS 3
518 times and then incubated with Alexa Fluor 546 goat anti-rabbit secondary antibody (Invitrogen
519 A-11035) diluted 1:250 in PBS containing 2% BSA for 1 h. Samples were washed 3 times in
520 PBS and stored in 1 ml PBS for imaging. N > 1000 cells were analyzed per condition. For

521 imaging, we used an inverted Nikon Diaphot 200 with a CCD camera (Andor Technologies) and
522 a 40X air Plan Fluor NA 0.60 or a 100X oil objective. The microscope was controlled by the
523 MicroManager software package (101). For differential immunostaining, all "green" bacteria
524 associated with individual cells were counted as adherent; bacteria that were both "green" and
525 "red" (due to antibody binding) were counted as non-internalized. Nuclei number was identified
526 running a custom-made script in MATLAB (Mathworks Inc.) and the CellC software was used for
527 enumeration of the bacteria (102). For characterization of total bacteria adhering to host cells
528 (Lm or Li), same procedure was followed with the exception that cells were permeabilized for 5
529 min in 0.2% Triton-X in PBS. Primary antibody used was goat polyclonal BacTrace anti-*Listeria*
530 genus specific antibody.
531
532 **Immunostaining of surface vimentin**
533 HMEC-1 cells residing on glass collagen I-coated coverslips were incubated at 37°C for
534 30 min with H-84 anti-vimentin antibody in 1:10 dilution in media. Cells were then washed three
535 times in PBS and fixed in 4% formaldehyde (EM grade) in PBS for 10 min at room temperature.
536 A blocking step with 5% FBS in PBS was followed for 30 min and then cells were incubated with
537 secondary goat anti-rabbit AlexaFluor-546 antibody diluted 1:250 in PBS containing 2% BSA for
538 1 h. For negative controls to ensure label is specific to primary antibody, cells with no primary
539 antibody were fixed and incubated for 1 h with secondary goat anti-rabbit AlexaFluor-546
540 antibody. As an additional control, cells were also fixed, permeabilized and stained for
541 intracellular vimentin. For imaging, we used an inverted Nikon Diaphot 200 with a CCD camera
542 (Andor Technologies) and a 100X oil objective.
543
544 **HMEC-1 cell transfection with siRNA**
545 For each well of a 24-well plate, $6x10^4$ HMEC-1 cells suspended in serum free media
546 were reverse-transfected with siRNAs at 20 nM final concentration using 0.25 μL lipofectamine

547 RNAiMAX (Invitrogen 13778075). The transfection mix was replaced by full media 8 h later.
548 Synthetic siRNA to target vimentin was purchased from Dharmacon. . HMEC-1 cells were
549 treated with control (non-targeting, siGLO and Kif11) or experimental siRNA as described in S2
550 Table. Specifically, to demonstrate that transfection performed was sufficient to get siRNAs into
551 the cells, we transfected cells with synthetic siRNA, siGLO, that makes cell exposed to it
552 fluorescent 24 h post-transfection (Table S2). In addition to track a cell cycle phenotype to verify
553 that knockdown has occurred with our protocol, we transfected cells with siKif11 that results in
554 substantial cell death of transfected cells, approximately 24-48 h post-transfection and can be
555 verified on the TC scope (Table S2). Infections were performed approximately 72 h after
556 transfection
557
558 **RT-qPCR**
559 HMEC-1 cells were treated with control or experimental siRNA as described above.
560 mRNA was harvested using the RNeasy Micro Kit (Qiagen, 74004) and cDNA was prepared
561 using the Superscript III First-strand Synthesis SuperMix (ThermoFisher, 18080–400). qPCR
562 was performed using TaqMan PreAmp Master (Thermofisher, 4331182). Genes of interest
563 were amplified using primers Hs00958113_g1 for Vimentin (ThermoFisher, 4331182) and
564 Hs99999905_m1 for GAPDH (ThermoFisher, 4333764) on a StepOnePlus Real-Time PCR
565 System. Normalized relative quantity (NRQ) and error were calculated as previously described
566 [92]. GAPDH was used as control gene.
567
568 **Western blotting of FAK and Met for HMEC-1 lysates coming from cells residing on**
569 **different substrates**
570 For assessing FAK and Met phosphorylation and expression levels, cells were seeded
571 on different substrates for 24 h, and then lysed with a buffer containing 1% Nonidet P-40, 0.5%
572 sodium deoxycholate, and a protease inhibitor mixture (PMSF, leupeptin, aprotinin, and sodium

573 orthovanadate). The total cell lysate was separated by SDS/PAGE (10% running, 4% stacking)
574 and transferred onto a nitrocellulose membrane (Immobilon P, 0.45-µm pore size). The
575 membrane was then incubated with the designated antibodies. Immunodetection was performed
576 using the Western-Light chemiluminescent detection system (Applied Biosystems).
577
578 **Cell surface protein isolation**
579 The isolation of cell surface proteins was adapted according to (103) and (104). Cells
580 were plated on 10 x 15 cm cell culture dishes until reaching confluency for each condition. Cells
581 from 10 dishes were incubated with vehicle control (DMSO) containing media and cells from
582 other 10 dishes with 2 µM PF537228 FAK inhibitor for 1 h. Cells were then washed three times
583 with DPBS+ (PBS, 0.901 mM CaCl2, 0.492 mM $MgCl_2$, 2.667 mM KCl, 1.47 mM KH_2PO_4,
584 137.931 mM NaCl, 8.060 mM Na_2HPO_4-$7H_2O$, 5.555 mM D-Glucose, 0.327 mM Sodium
585 Pyruvate), and incubated for 30 min with 0.5 mM EZ-Link Sulfo-NHS-SS-Biotin (APExBIO,
586 21331) in DPBS+ at 4°C. To quench any non-reacted biotinylation, 1 M Tris pH 8.0 at a final
587 concentration of 50 mM was added on each plate for 10 min at 4°C. The solution was then
588 discarded and plates were rinsed twice in 1X TBS (50 mM Tris-Cl pH 7.2, 150 mM NaCl). 2 ml
589 of TBS pH 7.2 with 1X protease inhibitor cocktail (1 mM EDTA, 10 µM E-64, 2 µg/ml leupeptin,
590 15 µg/ml benzamidine, 0.1 mM PMSF) and with 1X phosphatase inhibitor cocktail (1 mM
591 Na_3VO_4, 1 mM NaF) were added to each dish and cells were scraped into 40 ml falcon tubes.
592 Tubes were spun at 400 x g for 5 min and the supernatant was discarded. 10 ml of lysis buffer
593 (50 mM Tris-HCL pH 8.5, 150 mM NaCl, 2% NP-40, 0.25% Deoxycholate, 2x protease inhibitor
594 cocktail, 1x osphatase inhibitor cocktail) were added to each single pellet obtained from 10 x 15
595 cm plates, and cells were passed through a 25 G needle attached to a 10 ml syringe 3
596 times. Lysates were then sonicated for 5 min in a bioruptor with 30 sec ON/OFF cycle. 1 mM
597 $MgCl_2$ and 50 U/ml benzonase (Sigma, 9025-65-4) were added to the samples that were then
598 incubated at 4 °C for 2 h on a rotator. EDTA to a final concentration of 5 mM was added to each

599 sample and samples were spun in an ultracentrifuge (Rotor type 70.1 Ti; 33,000 rpm) at
600 100,000 x g for 60 min at 4 °C. Supernatants were then transferred into fresh 15 ml Falcon
601 tubes and protein concentration was estimated by the BCA protein assay (Thermo Fisher
602 Scientific, Pierce Rockford). Equal amounts of protein (~5 mg) from each extract were used for
603 cell surface protein isolation.
604 Streptavidin agarose beads (Pierce, 20347) were washed three times with lysis buffer.
605 50 µl per 5 mg/lysate were added for 2 h or overnight at 4 °C on a rotator. Samples were then
606 transferred to 2 ml gravity flow columns (BioRad) pre-equilibrated with 2 ml wash buffer I (50
607 mM Tris-HCL pH 8.5, 150 mM NaCl, 2% NP-40, 0.25% Deoxycholate, 0.5% SDS). The flow-
608 through was collected and stored at -80 °C. Columns were washed once with 2 ml lysis buffer
609 (excluding protease and phosphatase inhibitors), then with 2 ml wash buffer I, followed by a 2
610 ml wash with wash buffer II (50 mM Tris-HCL pH 8.5, 300 mM NaCl, 2% NP-40, 0.25%
611 Deoxycholate, 0.5% SDS) and then again with 2 ml wash buffer I. Beads were then transferred
612 to a fresh 1.5 ml Eppendorf tube and 3x volume of elution buffer (100 mM Tris-HCl pH 8.5, 2%
613 SDS, 100 mM DTT) was added and samples were incubated at 37 °C for 1 h on a thermomixer.
614 Beads were then spun down and supernatant was collected and 5% aliquoted for gel-analysis
615 (2.5% elution for Western Blot and 2.5% elution for Silver staining of 1D-PAGE gels) and the
616 rest was put in a fresh 1.5 ml Eppendorf tube and stored at -80°C.
617
618 **2D SDS-PAGE electrophoresis and staining**
619 Two-dimensional electrophoresis was performed according to the carrier ampholyte
620 method of isoelectric focusing (105, 106) by Kendrick Labs, Inc. (Madison, WI) as follows:
621 Isoelectric focusing was carried out in a glass tube of inner diameter 2.3 mm using 2% pH 3-10
622 Isodalt Servalytes (Serva, Heidelberg, Germany) for 9600 volt-h. 1 µg of an IEF internal
623 standard, tropomyosin, was added to the sample. This protein migrates as a doublet with lower
624 polypeptide spot of MW 33,000 and pI 5.2. The enclosed tube gel pH gradient plot for this set of

625 Servalytes was determined with a surface pH electrode. After equilibration for 10 min in Buffer
626 'O' (10% glycerol, 50 mM dithiothreitol, 2.3% SDS and 0.0625 M Tris, pH 6.8), each tube gel
627 was sealed to the top of a stacking gel that overlaid a 10% acrylamide slab gel (0.75 mm thick).
628 SDS slab gel electrophoresis was carried out for about 4 h at 15 mA/gel. The following proteins
629 (Sigma Chemical Co., St. Louis, MO and EMD Millipore, Billerica, MA) were used as molecular
630 weight standards: myosin (220,000), phosphorylase A (94,000), catalase (60,000), actin
631 (43,000), carbonic anhydrase (29,000) and lysozyme (14,000). These standards appear along
632 the basic edge of the silver-stained (107) 10% acrylamide slab gel. The gels were dried
633 between sheets of cellophane with the acid edge to the left.
634
635 **Manual comparisons of patterns of silver-stained 2D gels**
636 Each gel for comparison was overlaid with a transparent sheet for labeling polypeptide
637 spot differences without marking the original gel. Two experienced analysts manually compared
638 protein patterns and polypeptide spots that were unique to or differed between controls and
639 PF537228 samples were outlined.
640
641 **Protein digestion and peptide extraction**
642 Proteins that were separated by SDS-PAGE/2D-PAGE and stained by Coomassie dye
643 were excised, washed and the proteins from the gel were treated according to published
644 protocols (108-110). Briefly, the gel pieces were washed in high purity, high performance liquid
645 chromatography HPLC grade water, dehydrated and cut into small pieces and de-stained by
646 incubating in 50 mM ammonium bicarbonate, 50 mM ammonium bicarbonate/50% acetonitrile,
647 and 100% acetonitrile under moderate shaking, followed by drying in a speed-vac concentrator.
648 The gel bands were then rehydrated with 50 mM ammonium bicarbonate. The procedure was
649 repeated twice. The gel bands were then rehydrated in 50 mM ammonium bicarbonate
650 containing 10 mM DTT and incubated at 56°C for 45 minutes. The DTT solution was then

651 replaced by 50 mM ammonium bicarbonate containing 100 mM Iodoacetamide for 45 minutes in
652 the dark, with occasional vortexing. The gel pieces were then re-incubated in 50 mM ammonium
653 bicarbonate/50% acetonitrile, and 100% acetonitrile under moderate shaking, followed by drying
654 in speed-vac concentrator. The dry gel pieces were then rehydrated using 50 mM ammonium
655 bicarbonate containing 10 ng/ml trypsin and incubated overnight at 37°C under low shaking.
656 The resulting peptides were extracted twice with 5% formic acid/50 mM ammonium
657 bicarbonate/50% acetonitrile and once with 100% acetonitrile under moderate shaking. Peptide
658 mixture was then dried in a speed-vac, solubilized in 20 ml of 0.1% formic acid/2% acetonitrile.
659

660 **Liquid chromatography and tandem mass spectrometry (LC-MS/MS)**

661 The peptide mixture was analyzed by reverse phase liquid chromatography (LC) and MS
662 (LC-MS/MS) using a NanoAcuity UPLC (Micromass/Waters, Milford, MA) coupled to a Q-TOF
663 Ultima API MS (Micromass/Waters, Milford, MA), according to published procedures (108, 111-
664 113). Briefly, the peptides were loaded onto a 100 mm x 10 mm NanoAquity BEH130 C18 1.7
665 mm UPLC column (Waters, Milford, MA) and eluted over a 150 minute gradient of 2-80%
666 organic solvent (ACN containing 0.1% FA) at a flow rate of 400 nL/min. The aqueous solvent
667 was 0.1% FA in HPLC water. The column was coupled to a Picotip Emitter Silicatip nano-
668 electrospray needle (New Objective, Woburn, MA). MS data acquisition involved survey MS
669 scans and automatic data dependent analysis (DDA) of the top three ions with the highest
670 intensity ions with the charge of 2+, 3+ or 4+ ions. The MS/MS was triggered when the MS
671 signal intensity exceeded 10 counts/second. In survey MS scans, the three most intense peaks
672 were selected for collision-induced dissociation (CID) and fragmented until the total MS/MS ion
673 counts reached 10,000 or for up to 6 seconds each. The entire procedure used was previously
674 described (108, 111, 112). Calibration was performed for both precursor and product ions using
675 1 pmol GluFib (Glu1-Fibrinopeptide B) standard peptide with the sequence
676 EGVNDNEEGFFSAR and the monoisotopic doubly-charged peak with m/z of 785.84.

677

678 **LC-MS/MS data processing and protein identification**

679 The raw data were processed using ProteinLynx Global Server (PLGS, version 2.4)
680 software as previously described (111). The following parameters were used: background
681 subtraction of polynomial order 5 adaptive with a threshold of 30%, two smoothings with a
682 window of three channels in Savitzky-Golay mode and centroid calculation of top 80% of peaks
683 based on a minimum peak width of 4 channels at half height. The resulting pkl files were
684 submitted for database search and protein identification to the public Mascot database search
685 (www.matrixscience.com, Matrix Science, London, UK) using the following parameters:
686 databases from NCBI (bacteria), parent mass error of 1.3 Da, product ion error of 0.8 Da,
687 enzyme used: trypsin, one missed cleavage, propionamide as cysteine fixed modification and
688 Methionine oxidized as variable modification. To identify false negative results, we used
689 additional parameters such as different databases or organisms, a narrower error window for
690 the parent mass error (1.2 and then 0.2 Da) and for the product ion error (0.6 Da), and up to two
691 missed cleavage sites for trypsin. In addition, the pkl files were also searched against in-house
692 PLGS database version 2.4 (www.waters.com) using searching parameters similar to the ones
693 used for Mascot search. The Mascot and PLGS database search provided a list of proteins for
694 each gel band. To eliminate false positive results, for the proteins identified by either one
695 peptide or a mascot score lower than 25, we verified the MS/MS spectra that led to identification
696 of a protein.

697

698 **Atomic force microscopy force-distance measurements for hydrogel stiffness**
699 **characterization**

700 AFM force-distance beating were performed on PA hydrogel samples in 50mM HEPES
701 pH 7.5 buffer with a Park NX-10 AFM (Park Systems, Santa Clara, CA) using commercial silicon
702 nitride cantilevers CP-PNP-SiO with a sphere tip (sQube, 0.08 N/m stiffness, sphere radius ~ 1

703 micron) and gold coating on the reflective side. Temperature has been kept at 37 ˚C throughout
704 the experiment. Tip calibration curves were performed on glass substrate surface, which was
705 considered infinitely hard for the soft tips used. Two approach-withdraw cycles were performed
706 per cell. Data analysis of FD curves and calculation of Young's modulus was performed using
707 XEI software (Park Systems, Santa Clara, CA) and SPIP software (Image Metrology, Hørsholm,
708 Denmark).
709
710 **Visualization and comparison of distributions**
711 Distributions were visualized by using boxplots with the features indicated below. Bold
712 black line parallel to the x-axis indicates the median (second quartile) of the distribution and
713 boxplot's notched section shows the 95% confidence interval around the median (Wilcoxon–
714 Mann–Whitney nonparametric test). Regular black lines extended vertically below and above
715 the medians represent the first and third quartiles of the distribution. Lines extending vertically
716 from the boxplot (whiskers) represent the lowest datum within 1.5 IQR (interquartile range) of
717 the lower quartile and the highest datum within 1.5 IQR of the upper quartile. Outliers are
718 represented by circles. To assess whether the differences between the medians of two
719 distributions are significant we run a nonparametric Wilcoxon rank sum test since the
720 distributions are not normal. One or two asterisks denote statistically significant differences
721 between the medians of two distributions (<0.05 or <0.01, respectively).
722

723 **AUTHOR CONTRIBUTIONS:**

724 E.E.B. and J.A.T. conceived the project and designed the experiments. E.E.B. performed
725 experiments and analyzed data. Y.Y. performed experiments. E.E.B. and J.A.T. wrote the
726 paper.

727

728 **ACKNOWLEDGEMENTS:**

729 Our thanks to M. Footer, R. Lamason, M. Rengaranjan and members of the Theriot Lab for
730 discussions and experimental support. This work was supported by NIH R01AI036929 (J.A.T),
731 HHMI (J.A.T) and the American Heart Association (E.E.B. and Y.Y.). Flow cytometry was
732 performed at the Stanford Shared FACS Facility and RT-qPCR was performed at Stanford PAN
733 Facility.

734

735 **FIGURE LEGENDS**

736 **Figure 1. Uptake of Lm by HMEC-1 depends on the stiffness of the matrix on which cells**
737 **reside.**

738 HMEC-1 residing on PA hydrogels of varying stiffness coated with collagen I were infected with
739 Δ*actA* Lm (actAp::mTagRFP). Infection was analyzed by flow cytometry 7–8 h post infection.
740 Bacteria were added at a multiplicity of infection (MOI) between 30 to 50 bacteria per host cell.
741 **(A-D)** Histograms of the logarithm of bacterial fluorescence intensity per cell for HMEC-1 plated
742 on 0.6 kPa **(A)**, 3 kPa **(B)**, 20 kPa **(C)** and 70 kPa **(D)** PA hydrogels. Histograms for N=5
743 replicates are shown in different colors. Histogram of control uninfected cells is shown in purple.
744 Based on the autofluorescence of the control group a gate is defined (see black and red lines)
745 showing what is considered uninfected (left, black line) and infected (right, red line). **(E)**
746 Boxplots of percentage of HMEC-1 infected with Δ*actA* Lm versus hydrogel stiffness for the data
747 shown in panels A-D. Circles represent outliers, and the boxplots' notched sections show the
748 95% confidence interval around the median (Wilcoxon–Mann–Whitney test, for details about
749 boxplots see Materials and Methods). One or two asterisks denote statistically significant
750 differences between the medians of two distributions (<0.05 or <0.01, respectively; Wilcoxon
751 rank sum test). **(F)** Boxplots of normalized fraction of HMEC-1 infected with Δ*actA* Lm for cells
752 residing on PA hydrogels of varying stiffness or TC polystyrene. Stiffness (kPa) of each
753 substrate is indicated. Boxplots refer to data from 3 independent experiments, with N = 5-6
754 replicates per experiment. For each experiment values have been normalized relative to the
755 mean infection level of cells residing on polystyrene substrates.

756

757 **Figure 2. FAK activity of HMEC-1 residing on soft PA hydrogels is decreased, as is Lm**
758 **uptake.**

759 (**A)** Western blots from whole HMEC-1 lysates showing expression of phosphorylated FAK
760 (Tyr397) and total FAK for cells residing on soft gels (3 kPa), stiff gels (70 kPa) and TC

761 polystyrene substrates with or without 2 μM PF537228 FAK inhibitor. In each Western blot,
762 equal quantities of protein were loaded and equal loading was confirmed in relation to
763 glyceraldehyde 3-phosphate dehydrogenase (GAPDH) expression. In each case, the Western
764 blots shown are representative of 3 independent experiments. (**B-C)** Normalized ratio of
765 FAK/GAPDH **(B)** and pFAK (Tyr397)/GAPDH **(C)** for HMEC-1 residing on varying stiffness
766 substrates and treated or not with 2 μM PF537228 FAK inhibitor. Different color circles
767 correspond to data from 3 independent experiments. Black bars represent the mean of the 3
768 independent experiments. For each experiment values have been normalized relative to the
769 ratio for cells residing on polystyrene substrates. **(D)** Inhibition of bacterial uptake by FAK
770 inhibitors. FAK-14, PF573228 or vehicle control was added 1 h before addition of bacteria to
771 HMEC-1 residing on polystyrene substrates. Percentage of HMEC-1 infected with Δ*actA* Lm
772 (actAp::mTagRFP) as a function of inhibitor concentration (mean +/- SD, N = 4 replicates). Inset
773 shows the same data with concentration on a log scale. Infection was analyzed by flow
774 cytometry, 7–8 h after infection. MOI is 80. Representative data come from 1 of 3 independent
775 experiments.
776
777 **Figure 3. Lm adhesion but not invasion efficiency is increased when HMEC-1 reside on**
778 **stiff hydrogels.**
779 HMEC-1 residing on soft (3 kPa) or stiff (70 kPa) PA hydrogels and treated with vehicle control
780 or 2 μM PF537228 FAK inhibitor were infected with Lm (constitutively expressing GFP) at an
781 MOI between 1.5 to 15. 30 min post-infection samples were fixed, and immunostained, and
782 infection was analyzed by microscopy followed by image processing. Boxplots showing the
783 distribution of the normalized fraction of: (**A)** total bacteria per cell; **(B)** internalized bacteria per
784 cell; **(C)** invasion efficiency (ratio of internalized bacteria to total bacteria); **(D)** cells in the field of
785 view. For each experiment, values have been normalized relative to the mean value for cells
786 residing on stiff PA hydrogels without drug treatment. Boxplots refer to data from 3 independent

787 experiments and 2600-2900 cells were analyzed for each condition. Two asterisks denote
788 statistically significant differences between the medians of two distributions (<0.01; Wilcoxon
789 rank sum test).
790
791 **Figure 4. Infection of HMEC-1 by Lm is in part mediated by InlB in a manner independent**
792 **of matrix stiffness.**
793 (**A)** Percentage of HMEC-1 infected with Lm as a function of the logarithm of MOI (mean +/- SD,
794 N = 4 replicates). HMEC-1 were infected with the indicated strains: wild type (circle); Δ*inlA*
795 (square); Δ*inlB* (cross); Δ*inlF* (diamond) (actAp::mTagRFP). The frequency of infected HMEC-1
796 was determined by flow cytometry 7–8 h post infection. Representative data come from 1 of 3
797 independent experiments. (**B)** Percentage of HMEC-1 infected with Lm as a function of the
798 logarithm of MOI (mean +/- SD, N = 4 replicates). HMEC-1 were infected with the indicated
799 strains: Δ*actA* (black circle); Δ*actA/*Δ*inlB* (gray square) (actAp::mTagRFP). The frequency of
800 infected HMEC-1 was determined by flow cytometry 7–8 h post infection. Representative data
801 come from 1 of 3 independent experiments. **(C)** Boxplots of percentage of HMEC-1 infected with
802 Lm as a function of substrate stiffness (N = 5-6 replicates). HMEC-1 were infected with the
803 indicated Lm strains: Δ*actA* (gray); Δ*actA/*Δ*inlB* (black) (actAp::mTagRFP) at an MOI of 20.
804 Infection was analyzed by flow cytometry, 7–8 h after infection. Representative data come from
805 1 of 3 independent experiments. One or two asterisks denote statistically significant differences
806 between the medians of two distributions (<0.05 or <0.01, respectively; Wilcoxon rank sum test).
807 (**D-F)** HMEC-1 residing on collagen I-coated glass substrates were infected with Lm
808 (constitutively expressing GFP) or Δ*inlB* Lm at an MOI of 3.5. 30 min post-infection samples
809 were fixed, immunostained and infection was analyzed by microscopy followed by image
810 processing. Boxplots showing: (**D)** total bacteria per cell; **(E)** internalized bacteria per cell; **(F)**
811 invasion efficiency (ratio of internalized bacteria to total bacteria). For each condition, 500-550
812 cells were analyzed in total. **(G)** Percentage of HMEC-1 infected with Lm as a function of SGX-

813 523 Met inhibitor concentration (mean +/- SD, N = 4 replicates). SGX-523 or vehicle control was
814 added 1 h before addition of bacteria. HMEC-1 were infected with the indicated strains: Δ*actA*
815 (black circle); Δ*actA/*Δ*inlB* (gray square) (actAp::mTagRFP) at an MOI of 75. Infection was
816 analyzed by flow cytometry, 7–8 h after infection. Representative data come from 1 of 3
817 independent experiments. **(H)** Boxplots of percentage of HMEC-1 infected with Lm as a function
818 of substrate stiffness (N = 5-6 replicates). HMEC-1 were treated with vehicle control or 1 μM
819 SGX-523 Met inhibitor for 1 h prior to infection and then infected with Δ*actA* Lm
820 (actAp::mTagRFP). Infection was analyzed by flow cytometry, 7–8 h after infection. MOI is 20.
821 Representative data come from 1 of 3 independent experiments. **(I)** Percentage of HMEC-1
822 infected with Lm as a function of PF537228 inhibitor concentration (mean +/- SD, N = 4
823 replicates). PF537228 or vehicle control was added 1 h before addition of bacteria (see Suppl.
824 Fig. 1D). HMEC-1 were infected with the indicated strains: Δ*actA* (black circle); Δ*actA/*Δ*inlB*
825 (gray square) (actAp::mTagRFP) at an MOI of 75. Infection was analyzed by flow cytometry, 7–
826 8 h after infection. Representative data come from 1 of 3 independent experiments. Inset shows
827 the same data with concentration on a log scale.
828
829 **Figure 5. Lower FAK activity leads to reduced amount of cell surface vimentin.**
830 (**A-B)** 2D-PAGE gels of plasma membrane proteins of HMEC-1 grown on TC polystyrene
831 substrates treated for 1 h with vehicle control (**A)** or 2 μM PF537228 FAK inhibitor (**B).** pH
832 increases from left to right. Gels were silver stained and one isoelectric point marker
833 (tropomyosin), added to each sample as an internal standard, is marked with a black arrow. The
834 one spot that differed consistently between 3 independent experiments is indicated with a black
835 circle and corresponds to vimentin (55 kDa).
836
837 **Figure 6. Surface vimentin is localized along the periphery of HMEC-1.**

838 Cells were stained for vimentin using the rabbit anti-vimentin H-84 antibody. For negative
839 controls, cells were stained with secondary anti-rabbit IgG antibody alone. Representative
840 phase image of cells (Phase, left column), image of the nuclei (DAPI, middle column) and
841 antibody fluorescence (AF-546, right column) are shown for: (**A)** Permeabilized HMEC-1 treated
842 with vehicle control and strained for intracellular vimentin; (**B)** Permeabilized HMEC-1 treated
843 with 2 μM PF537228 FAK inhibitor and strained for intracellular vimentin. (**C)** Permeabilized
844 HMEC-1 treated with vehicle control and incubated with anti-rabbit IgG alone as negative
845 controls. (**D)** Non permeabilized HMEC-1 treated with vehicle control and stained for surface
846 vimentin; (**E)** Non permeabilized HMEC-1 treated with 2 μM PF537228 FAK inhibitor and
847 stained for surface vimentin. (**F)** Non permeabilized HMEC-1 treated with vehicle control and
848 incubated with anti-rabbit IgG alone as negative controls. Scale bar shown in white is 20 μm.
849 White arrows point at the localization of surface vimentin at cell-cell junctions.
850
851 **Figure 7. Surface vimentin of HMEC-1 is implicated in Lm uptake.** (**A)** Decrease in bacterial
852 uptake after blocking HMEC-1 with anti-vimentin antibody H-84. Barplots of normalized fraction
853 of HMEC-1 infected with Δ*actA* Lm (actAp::mTagRFP) as a function of antibody concentration
854 (means +/-S.D., 3 independent experiments and N=4 replicates per experiment). For each
855 experiment, values have been normalized relative to the mean infection level of cells treated
856 with isotype control. Infection was analyzed by flow cytometry, 7–8 h after infection. (**B)** Barplots
857 of normalized fraction of HMEC-1 infected with Δ*actA* Lm (actAp::mTagRFP) and treated either
858 with non-targeting siRNA (siNT) or vimentin siRNA (siVIM) (means +/-S.D., 3 independent
859 experiments and N=4-6 replicates per experiment). For each experiment values have been
860 normalized relative to the mean infection level of cells treated with siNT. (**C)** Decreased uptake
861 of Lm when HMEC-1 are treated with withaferin that captures soluble vimentin 30 min prior to
862 infection. Barplots show normalized fraction of HMEC-1 infected with Δ*actA* Lm
863 (actAp::mTagRFP) as a function of withaferin concentration (means +/-S.D., 3 independent

864 experiments and N=4 replicates per experiment). For each experiment, values have been
865 normalized relative to the mean infection level of cells treated with vehicle control. Infection was
866 analyzed by flow cytometry, 7–8 h after infection. One or two asterisks denote statistically
867 significant differences between the medians of infection fraction of control versus all other
868 groups (<0.05 or <0.01, respectively; Wilcoxon rank sum test). (**D**) Percentage of HMEC-1
869 infected with Lm as a function of the logarithm of MOI (mean +/- SD, N = 4 replicates). HMEC-1
870 were infected with the indicated strains: Δ*actA* (black); Δ*actA/*Δ*inlB* (gray) (actAp::mTagRFP)
871 and HMEC-1 were treated with vehicle control (circle) or withaferin (diamond) for 30 min prior to
872 infection. The frequency of infected HMEC-1 was determined by flow cytometry 7–8 h post
873 infection. Representative data come from 1 of 3 independent experiments. MOI if not indicated
874 ranged from 50 to 120.
875
876 **Figure 8. Blocking HMEC-1 with anti-vimentin antibody reduces Li adhesion onto HMEC-1**
877 **but not uptake of beads.**
878 **(A)** Boxplots showing the number of bacteria per cell, for HMEC-1 residing on glass substrates
879 and treated with vehicle control, 2 μM PF537228 FAK inhibitor, or 80 μg/ml H-84 anti-vimentin
880 antibody prior to infection. Cells were infected with Lm or Li at an MOI of 4. 30 min post-infection
881 samples were fixed, immunostained and adhesion of bacteria was analyzed by microscopy
882 followed by image processing. For each condition, 2300-2600 cells were analyzed in total and
883 data refer to 1 of 2 independent experiments. Two asterisks denote statistically significant
884 differences between the median values of control cells versus all other groups <0.01; Wilcoxon
885 rank sum test). **(B)** HMEC-1 residing on TC polystyrene substrates and blocked for 1 h with
886 varying concentrations of H-84 anti-vimentin antibody or isotype control were "infected" with 2
887 μm beads at different concentrations. The frequency of micro-bead uptake by HMEC-1 was
888 determined by flow cytometry 2 h post addition of beads. Plot shows percentage of cells that
889 internalized beads as a function of the log of beads/cell added for different H-84 antibody

890 concentrations (mean +/- SD, N = 4 replicates).

891

892 **SUPPORTING INFORMATION CAPTIONS**

893 **Figure S1. Lm infection of VECs residing on hydrogels of varying stiffness.**

894 **(A)** Young's moduli of hydrogels. Plot showing the expected Young's modulus of the hydrogels
895 given the amount of acrylamide and bis-acrylamide used versus the Young's modulus
896 measured through AFM (N=6). Stiffness of the 0.6 kPa could not be measured, as the
897 hydrogels were very soft and adhered to the AFM tip. **(B)** Fraction of cells passed through the
898 flow cell in 20 s for HMEC-1 residing on varying stiffness substrates. HMEC-1 were seeded on
899 0.6 kPa, 3 kPa, 20 kPa and 70 kPa PA hydrogels as well as TC polystyrene substrates for 24 h
900 at a starting concentration of $4x10^5$ cells per well for 24 h. Cells were then detached from their
901 matrix and number of cells per well passed through the flow cell in 20 s was measured using a
902 flow cytometry for cells coming from N=5-6 wells for each substrate stiffness. Results from 3
903 independent experiments were combined and for each experiment values were normalized
904 relative to the mean number of cells passed through the flow cell for cells residing on TC
905 polystyrene substrates. No significant differences were detected. **(C)** Western blot from whole
906 HMEC-1 lysates showing expression of Met for cells seeded on soft (3 kPa), stiff (70 kPa) and
907 TC polystyrene substrates treated or not with 2 μM PF537228 FAK inhibitor. In each case, equal
908 quantities of protein were loaded and equal loading was also confirmed in relation to
909 glyceraldehyde 3-phosphate dehydrogenase (GAPDH) expression.

910

911 **Figure S2. Substrate stiffness and FAK activity decrease in bacterial uptake independent**
912 **of InlB. (A)** Boxplots of normalized fraction of HMEC-1 infected with Lm as a function of
913 substrate stiffness. Boxplots refer to data from 3 independent experiments, with N = 5-6
914 replicates per experiment. For each experiment, values have been normalized relative to the
915 mean infection level of cells residing on polystyrene substrates. HMEC-1 were infected with the
916 indicated Lm strains: Δ*actA* (gray); Δ*actA*/Δ*inlB* (black) (actAp::mTagRFP). Infection was
917 analyzed by flow cytometry, 7–8 h after infection. MOI is between 20 to 75. One or two asterisks

918 denote statistically significant differences between the medians of two distributions (<0.05 or
919 <0.01, respectively; Wilcoxon rank sum test). **(B)** Boxplots of normalized fraction of HMEC-1
920 infected with Lm as a function of substrate stiffness (N = 5-6 replicates). HMEC-1 were treated
921 with vehicle control (black) or 1 μM SGX-523 Met inhibitor (gray) for 1 h prior to infection and
922 then infected with Δ*actA* Lm (actAp::mTagRFP). Boxplots refer to data coming from 3
923 independent experiments, with N = 5-6 biological replicates per experiment. For each
924 experiment, values have been normalized relative to the mean infection level of cells residing on
925 polystyrene substrates. Infection was analyzed by flow cytometry, 7–8 h after infection. MOI is
926 between 25 to 50.
927
928 **Figure S3. Blocking HMEC-1 with anti-vimentin antibody or treating HMEC-1 with**
929 **withaferin reduces Lm uptake up to two-fold.** (A) Percentage of HMEC-1 infected with Δ*actA*
930 Lm (actAp::mTagRFP) when cells are blocked with varying H-84 anti-vimentin antibody
931 concentrations. Barplots represent means +/-S.D. and N=6 replicates. Isotype control (IgG) is
932 also shown. Infection was analyzed by flow cytometry, 7–8 h after infection. MOI is 90. Two
933 asterisks denote statistically significant differences between the medians of isotype control
934 versus all other groups (<0.01; Wilcoxon rank sum test). (**B)** InlB and surface vimentin both
935 contribute to uptake of Lm by HMEC-1. Barplots of normalized fraction of HMEC-1 infected with
936 either Δ*actA* (black) or Δ*actA/*Δ*inlB* (gray) Lm (actAp::mTagRFP) and treated with vehicle
937 control or 5 μM withaferin (means +/-S.D., 3 independent experiments and N=4 replicates per
938 experiment). For each experiment, values have been normalized relative to the mean infection
939 level of cells treated with vehicle control and infected with Δ*actA* Lm. The frequency of infected
940 HMEC-1 was determined by flow cytometry 7–8 h post infection. MOI if not indicated ranged
941 from 50 to 120.
942
943 **Figure S4. Knocking down vimentin decreases Lm uptake.** (**A-B)** Histograms of the

944 logarithm of Lm fluorescence intensity per cell for HMEC-1 treated with 20 nM of non-targeting
945 siRNA (siNT) **(A)** or vimentin siRNA (siVIM) **(B)**. HMEC-1 were infected with *ΔactA* Lm
946 (actAp::mTagRFP) and infection was analyzed by flow cytometry, 7–8 h after infection. MOI is
947 34. Histograms for N=6 replicates are shown in different colors. Control uninfected cells'
948 histogram is shown in purple. Based on the autofluorescence of the control group a gate is
949 defined (see black and red lines) showing what is considered uninfected (left, black line) and
950 infected (right, red line). **(C)** Number of HMEC-1 passed through the flow cell in 20 s, for N = 4
951 samples coming from wells treated with either siNT or siVIM. **(D)** Boxplots of percentage of
952 HMEC-1 infected with *ΔactA* Lm for the data shown in panels A-B. One or two asterisks denote
953 statistically significant differences between the medians of two distributions (<0.05 or <0.01,
954 respectively; Wilcoxon rank sum test). **(E)** Relative with respect to GAPDH gene expression of
955 vimentin obtained by RT-qPCR. The levels relative levels of expression in each siRNA treated
956 sample (#1-#3) are expressed relative to the control siNT treated sample #2 (normalized relative
957 quantity, NRQ). N=3 replicates are shown for each group treated with either siNT or siVIM.
958
959 **SUPPLEMENTARY TABLES**
960 **Supplementary Table 1. Bacterial strains used in this study.**
961 **Supplementary Table 2. Synthetic siRNA pools used in this study.**
962

REFERENCES

1. Lemichez E, Lecuit M, Nassif X, Bourdoulous S. Breaking the wall: targeting of the endothelium by pathogenic bacteria. Nat Rev Micro. 2010;8(2):93-104.
2. Wood JA, Shah NM, McKee CT, Hughbanks ML, Liliensiek SJ, Russell P, et al. The role of substratum compliance of hydrogels on vascular endothelial cell behavior. Biomaterials. 2011;32(22):5056-64.
3. Liliensiek SJ, Wood JA, Yong J, Auerbach R, Nealey PF, Murphy CJ. Modulation of Human Vascular Endothelial Cell Behaviors by Nanotopographic Cues. Biomaterials. 2010;31(20):5418-26.
4. Barakat AI, Lieu DK. Differential responsiveness of vascular endothelial cells to different types of fluid mechanical shear stress. Cell Biochemistry and Biophysics. 2003;38(3):323-43.
5. Ostrowski Maggie A, Huang Ngan F, Walker Travis W, Verwijlen T, Poplawski C, Khoo Amanda S, et al. Microvascular Endothelial Cells Migrate Upstream and Align Against the Shear Stress Field Created by Impinging Flow. Biophysical Journal. 2014;106(2):366-74.
6. Chien S, Li S, Shiu YT, Li YS. Molecular basis of mechanical modulation of endothelial cell migration. Front Biosci. 2005;10:1985-2000.
7. Yeh Y-T, Hur SS, Chang J, Wang K-C, Chiu J-J, Li Y-S, et al. Matrix Stiffness Regulates Endothelial Cell Proliferation through Septin 9. PLoS ONE. 2012;7(10):e46889.
8. Krishnan R, Klumpers DD, Park CY, Rajendran K, Trepat X, van Bezu J, et al. Substrate stiffening promotes endothelial monolayer disruption through enhanced physical forces. American Journal of Physiology - Cell Physiology. 2011;300(1):C146-C54.
9. Collins C, Osborne LD, Guilluy C, Chen Z, O'Brien ET, Reader JS, et al. Haemodynamic and extracellular matrix cues regulate the mechanical phenotype and stiffness of aortic endothelial cells. Nature Communications. 2014;5:3984.
10. Volkman BF, Prehoda KE, Scott JA, Peterson FC, Lim WA. Structure of the N-WASP EVH1 domain-WIP complex: insight into the molecular basis of Wiskott-Aldrich syndrome. Cell. 2002;111:565-76.
11. Wood JA, Liliensiek SJ, Russell P, Nealey PF, Murphy CJ. Biophysical Cueing and Vascular Endothelial Cell Behavior. Materials. 2010;3(3).
12. Kohn JC, Lampi MC, Reinhart-King CA. Age-related vascular stiffening: causes and consequences. Frontiers in Genetics. 2015;6:112.
13. Janmey PA, Miller RT. Mechanisms of mechanical signaling in development and disease. Journal of Cell Science. 2011;124(1):9-18.
14. Wells RG. The role of matrix stiffness in regulating cell behavior. Hepatology. 2008;47(4):1394-400.
15. Onken MD, Mooren OL, Mukherjee S, Shahan ST, Li J, Cooper JA. Endothelial Monolayers and Transendothelial Migration Depend on Mechanical Properties of the Substrate. Cytoskeleton (Hoboken). 2014;71(12):695-706.
16. Schwartz MA. Integrins and Extracellular Matrix in Mechanotransduction. Cold Spring Harbor Perspectives in Biology. 2010;2(12):a005066.
17. Senger DR, Perruzzi CA, Streit M, Koteliansky VE, de Fougerolles AR, Detmar M. The α(1)β(1) and α(2)β(1) Integrins Provide Critical Support for Vascular Endothelial Growth Factor Signaling, Endothelial Cell Migration, and Tumor Angiogenesis. The American Journal of Pathology. 2002;160(1):195-204.
18. Pelham RJ, Wang YI. Cell locomotion and focal adhesions are regulated by substrate flexibility. Proc Natl Acad Sci U S A. 1997;94(25):13661.
19. Du J, Zu Y, Li J, Du S, Xu Y, Zhang L, et al. Extracellular matrix stiffness dictates Wnt expression through integrin pathway. Scientific Reports. 2016;6:20395.

20. Provenzano PP, Inman DR, Eliceiri KW, Keely PJ. Matrix density-induced mechanoregulation of breast cell phenotype, signaling, and gene expression through a FAK-ERK linkage. Oncogene. 2009;28(49):4326-43.
21. Khatiwala CB, Peyton SR, Putnam AJ. Intrinsic mechanical properties of the extracellular matrix affect the behavior of pre-osteoblastic MC3T3-E1 cells. American Journal of Physiology - Cell Physiology. 2006;290(6):C1640.
22. Higuita-Castro N, Mihai C, Hansford DJ, Ghadiali SN. Influence of airway wall compliance on epithelial cell injury and adhesion during interfacial flows. Journal of Applied Physiology. 2014;117(11):1231-42.
23. Trepat X, Lenormand G, Fredberg JJ. Universality in cell mechanics. Soft Matter. 2008;4(9):1750-9.
24. Birukova AA, Tian X, Cokic I, Beckham Y, Gardel M, Birukov KG. Endothelial barrier disruption and recovery is controlled by substrate stiffness. Microvascular research. 2013;87:50-7.
25. Vazquez-Boland JA, Kuhn M, Berche P, Chakraborty T, Dominguez-Bernal G, Goebel W, et al. Listeria pathogenesis and molecular virulence determinants. Clin Microbiol Rev. 2001;14(3):584-640.
26. Jackson KA, Iwamoto M, Swerdlow D. Pregnancy-associated listeriosis. Epidemiol Infect. 2010;138(10):1503-9.
27. Parida SK, Domann E, Rohde M, Muller S, Darji A, Hain T, et al. Internalin B is essential for adhesion and mediates the invasion of Listeria monocytogenes into human endothelial cells. Mol Microbiol. 1998;28(1):81-93.
28. Bierne H, Cossart P. InlB, a surface protein of Listeria monocytogenes that behaves as an invasin and a growth factor. Journal of Cell Science. 2002;115(17):3357.
29. Gundelfinger ED, Kessels MM, Qualmann B. Temporal and spatial coordination of exocytosis and endocytosis. Nature Rev Mol Cell Biol. 2003;4:127-39.
30. Kirchner M, Higgins DE. Inhibition of ROCK activity allows InlF-mediated invasion and increased virulence of Listeria monocytogenes. Mol Microbiol. 2008;68(3):749-67.
31. Tilney LG, Portnoy DA. Actin filaments and the growth, movement, and spread of the intracellular bacterial parasite, Listeria monocytogenes. The Journal of Cell Biology. 1989;109(4):1597-608.
32. Gaillard JL, Berche P, Mounier J, Richard S, Sansonetti P. In vitro model of penetration and intracellular growth of Listeria monocytogenes in the human enterocyte-like cell line Caco-2. Infection and Immunity. 1987;55(11):2822-9.
33. Dabiri GA, Sanger JM, Portnoy DA, Southwick FS. Listeria monocytogenes moves rapidly through the host-cell cytoplasm by inducing directional actin assembly. Proceedings of the National Academy of Sciences of the United States of America. 1990;87(16):6068-72.
34. Theriot J, Mitchison T, Tilney L, Portnoy D. The rate of actin-based motility of intracellular Listeria monocytogenes equals the rate of actin polymerization. Nature. 1992;357(6375):257-60.
35. Kocks C, Gouin E, Tabouret M, Berche P, Ohayon H, Cossart P. L. monocytogenes-induced actin assembly requires the actA gene product, a surface protein. Cell. 1992;68(3):521-31.
36. Drevets DA, Sawyer RT, Potter TA, Campbell PA. Listeria monocytogenes infects human endothelial cells by two distinct mechanisms. Infect Immun. 1995;63(11):4268-76.
37. Wilson SL, Drevets DA. Listeria monocytogenes infection and activation of human brain microvascular endothelial cells. J Infect Dis. 1998;178(6):1658-66.
38. Pizarro-Cerdá J, Cossart P. Bacterial Adhesion and Entry into Host Cells. Cell. 2006;124(4):715-27.
39. Clarke EJ, Allan V. Intermediate filaments: vimentin moves in. Curr Biol. 2002;12.

40. Päll T, Pink A, Kasak L, Turkina M, Anderson W, Valkna A, et al. Soluble CD44 Interacts with Intermediate Filament Protein Vimentin on Endothelial Cell Surface. PLOS ONE. 2011;6(12):e29305.
41. Mitra A, Satelli A, Xia X, Cutrera J, Mishra L, Li S. Cell-surface Vimentin: A mislocalized protein for isolating csVimentin(+) CD133(-) novel stem-like hepatocellular carcinoma cells expressing EMT markers. International journal of cancer. 2015;137(2):491-6.
42. Shigyo M, Kuboyama T, Sawai Y, Tada-Umezaki M, Tohda C. Extracellular vimentin interacts with insulin-like growth factor 1 receptor to promote axonal growth. Scientific Reports. 2015;5:12055.
43. Mor-Vaknin N, Punturieri A, Sitwala K, Markovitz DM. Vimentin is secreted by activated macrophages. Nat Cell Biol. 2003;5(1):59-63.
44. Rohrbeck A, Schroder A, Hagemann S, Pich A, Holtje M, Ahnert-Hilger G, et al. Vimentin mediates uptake of C3 exoenzyme. PLoS One. 2014;9(6):e101071.
45. Mak TN, Brüggemann H. Vimentin in Bacterial Infections. Cells. 2016;5(2):18.
46. Bhattacharya R, Gonzalez AM, DeBiase PJ, Trejo HE, Goldman RD, Flitney FW, et al. Recruitment of vimentin to the cell surface by β3 integrin and plectin mediates adhesion strength. Journal of Cell Science. 2009;122(9):1390.
47. Zou Y, He L, Huang SH. Identification of a surface protein on human brain microvascular endothelial cells as vimentin interacting with Escherichia coli invasion protein IbeA. Biochemical and biophysical research communications. 2006;351(3):625-30.
48. Garg A, Barnes PF, Porgador A, Roy S, Wu S, Nanda JS, et al. Vimentin expressed on Mycobacterium tuberculosis-infected human monocytes is involved in binding to the NKp46 receptor. J Immunol. 2006;177(9):6192-8.
49. Yang J, Zou L, Yang Y, Yuan J, Hu Z, Liu H, et al. Superficial vimentin mediates DENV-2 infection of vascular endothelial cells. Scientific Reports. 2016;6:38372.
50. Yu YT-C, Chien S-C, Chen IY, Lai C-T, Tsay Y-G, Chang SC, et al. Surface vimentin is critical for the cell entry of SARS-CoV. Journal of Biomedical Science. 2016;23(1):14.
51. Du N, Cong H, Tian H, Zhang H, Zhang W, Song L, et al. Cell Surface Vimentin Is an Attachment Receptor for Enterovirus 71. Journal of Virology. 2014;88(10):5816-33.
52. Dussurget O, Pizarro-Cerda J, Cossart P. Molecular determinants of Listeria monocytogenes virulence. Annu Rev Microbiol. 2004;58:587-610.
53. Sperling LH, Friedman DW. Synthesis and mechanical behavior of interpenetrating polymer networks: Poly(ethyl acrylate) and polystyrene. Journal of Polymer Science Part A-2: Polymer Physics. 1969;7(2):425-7.
54. Ahmed EM. Hydrogel: Preparation, characterization, and applications: A review. Journal of Advanced Research. 2015;6(2):105-21.
55. Mih JD, Sharif AS, Liu F, Marinkovic A, Symer MM, Tschumperlin DJ. A Multiwell Platform for Studying Stiffness-Dependent Cell Biology. PLoS ONE. 2011;6(5):e19929.
56. Georges P, Miller W, Meaney D, Sawyer E, Janmey PA. Matrices with compliance comparable to that of brain tissue select neuronal over glial growth in mixed cortical cultures. Biophys J. 2006;90(8):3012-8.
57. Huang C, Butler PJ, Tong S, Muddana HS, Bao G, Zhang S. Substrate stiffness regulates cellular uptake of nanoparticles. Nano letters. 2013;13(4):1611-5.
58. Yeung T, Georges PC, Flanagan LA, Marg B, Ortiz M, Funaki M, et al. Effects of substrate stiffness on cell morphology, cytoskeletal structure, and adhesion. Cell Motil Cytoskeleton. 2005;60(1):24-34.
59. Tse JR, Engler AJ. Preparation of hydrogel substrates with tunable mechanical properties. Current protocols in cell biology. 2010;Chapter 10:Unit 10.6.
60. Zeldovich VB, Robbins JR, Kapidzic M, Lauer P, Bakardjiev AI. Invasive extravillous trophoblasts restrict intracellular growth and spread of Listeria monocytogenes. PLoS Pathog. 2011;7(3):e1002005.

61. Mathieu SV, Aragão KS, Imberty A, Varrot A. Discoidin I from Dictyostelium discoideum and interactions with oligosaccharides: specificity, affinity, crystal structures and comparison with Discoidin II. Journal of molecular biology. 2010;400(3):540-54.
62. Greiffenberg L, Goebel W, Kim KS, Weiglein I, Bubert A, Engelbrecht F, et al. Interaction of Listeria monocytogenes with human brain microvascular endothelial cells: InlB-dependent invasion, long-term intracellular growth, and spread from macrophages to endothelial cells. Infect Immun. 1998;66(11):5260-7.
63. Buchanan SG, Hendle J, Lee PS, Smith CR, Bounaud PY, Jessen KA, et al. SGX523 is an exquisitely selective, ATP-competitive inhibitor of the MET receptor tyrosine kinase with antitumor activity in vivo. Mol Cancer Ther. 2009;8(12):3181-90.
64. Nunomura K, Nagano K, Itagaki C, Taoka M, Okamura N, Yamauchi Y, et al. Cell surface labeling and mass spectrometry reveal diversity of cell surface markers and signaling molecules expressed in undifferentiated mouse embryonic stem cells. Molecular & cellular proteomics : MCP. 2005;4(12):1968-76.
65. Fujimoto T, Nakade S, Miyawaki A, Mikoshiba K, Ogawa K. Localization of inositol 1,4,5-trisphosphate receptor-like protein in plasmalemmal caveolae. J Cell Biol. 1992;119(6):1507-13.
66. Elia G. Cell surface protein biotinylation for SDS-PAGE analysis. Methods Mol Biol. 2012;869:361-72.
67. Fuchs E, Weber K. Intermediate filaments: structure, dynamics, function, and disease. Annu Rev Biochem. 1994;63:345-82.
68. Chi F, Jong TD, Wang L, Ouyang Y, Wu C, Li W, et al. Vimentin-mediated signalling is required for IbeA+ E. coli K1 invasion of human brain microvascular endothelial cells. Biochem J. 2010;427(1):79-90.
69. Bargagna-Mohan P, Deokule SP, Thompson K, Wizeman J, Srinivasan C, Vooturi S, et al. Withaferin A Effectively Targets Soluble Vimentin in the Glaucoma Filtration Surgical Model of Fibrosis. PLOS ONE. 2013;8(5):e63881.
70. Bargagna-Mohan P, Hamza A, Kim Y-e, Khuan Ho Y, Mor-Vaknin N, Wendschlag N, et al. The Tumor Inhibitor and Antiangiogenic Agent Withaferin A Targets the Intermediate Filament Protein Vimentin. Chemistry & Biology.14(6):623-34.
71. Glaser P, Frangeul L, Buchrieser C, Rusniok C, Amend A, Baquero F, et al. Comparative genomics of Listeria species. Science. 2001;294(5543):849-52.
72. Kohn Julie C, Zhou Dennis W, Bordeleau F, Zhou Allen L, Mason Brooke N, Mitchell Michael J, et al. Cooperative Effects of Matrix Stiffness and Fluid Shear Stress on Endothelial Cell Behavior. Biophysical Journal. 2015;108(3):471-8.
73. Li S, Kim M, Hu YL, Jalali S, Schlaepfer DD, Hunter T, et al. Fluid shear stress activation of focal adhesion kinase. Linking to mitogen-activated protein kinases. J Biol Chem. 1997;272(48):30455-62.
74. Zebda N, Dubrovskyi O, Birukov KG. Focal adhesion kinase regulation of mechanotransduction and its impact on endothelial cell functions. Microvascular research. 2012;83(1):71-81.
75. Koudelka KJ, Destito G, Plummer EM, Trauger SA, Siuzdak G, Manchester M. Endothelial targeting of cowpea mosaic virus (CPMV) via surface vimentin. PLoS Pathog. 2009;5.
76. Das S, Ravi V, Desai A. Japanese encephalitis virus interacts with vimentin to facilitate its entry into porcine kidney cell line. Virus Res. 2011;160.
77. Lebrun M, Mengaud J, Ohayon H, Nato F, Cossart P. Internalin must be on the bacterial surface to mediate entry of Listeria monocytogenes into epithelial cells. Mol Microbiol. 1996;21(3):579-92.
78. Lecuit M, Hurme R, Pizarro-Cerda J, Ohayon H, Geiger B, Cossart P. A role for alpha-and beta-catenins in bacterial uptake. Proc Natl Acad Sci U S A. 2000;97(18):10008-13.

79. Ise H, Kobayashi S, Goto M, Sato T, Kawakubo M, Takahashi M, et al. Vimentin and desmin possess GlcNAc-binding lectin-like properties on cell surfaces. Glycobiology. 2010;20(7):843-64.
80. Konopka JB. N-acetylglucosamine (GlcNAc) functions in cell signaling. Scientifica. 2012;2012.
81. Fiedler F. Biochemistry of the cell surface of Listeria strains: a locating general view. Infection. 1988;16 Suppl 2:S92-7.
82. Gopal S, Bober A, Whiteford JR, Multhaupt HA, Yoneda A, Couchman JR. Heparan sulfate chain valency controls syndecan-4 function in cell adhesion. J Biol Chem. 2010;285(19):14247-58.
83. Liu D, Shriver Z, Venkataraman G, El Shabrawi Y, Sasisekharan R. Tumor cell surface heparan sulfate as cryptic promoters or inhibitors of tumor growth and metastasis. Proceedings of the National Academy of Sciences. 2002;99(2):568-73.
84. Henry-Stanley MJ, Hess DJ, Erickson EA, Garni RM, Wells CL. Role of heparan sulfate in interactions of Listeria monocytogenes with enterocytes. Medical Microbiology and Immunology. 2003;192(2):107-15.
85. Kolewe KW, Peyton SR, Schiffman JD. Fewer Bacteria Adhere to Softer Hydrogels. ACS Appl Mater Interfaces. 2015;7(35):19562-9.
86. Tang X, Wen Q, Kuhlenschmidt TB, Kuhlenschmidt MS, Janmey PA, Saif TA. Attenuation of Cell Mechanosensitivity in Colon Cancer Cells during In Vitro Metastasis. PLoS ONE. 2012;7(11):e50443.
87. Ingram DA, Mead LE, Tanaka H, Meade V, Fenoglio A, Mortell K, et al. Identification of a novel hierarchy of endothelial progenitor cells using human peripheral and umbilical cord blood. Blood. 2004;104(9):2752-60.
88. Aird WC. Endothelial Cell Heterogeneity. Cold Spring Harbor Perspectives in Medicine. 2012;2(1).
89. Aird WC. Phenotypic heterogeneity of the endothelium: I. Structure, function, and mechanisms. Circ Res. 2007;100(2):158-73.
90. Aird WC. Endothelial Cell Heterogeneity. Cold Spring Harbor Perspectives in Medicine. 2012;2(1):a006429.
91. Ye M, Sanchez HM, Hultz M, Yang Z, Bogorad M, Wong AD, et al. Brain microvascular endothelial cells resist elongation due to curvature and shear stress. Scientific Reports. 2014;4:4681.
92. Stroka KM, Aranda-Espinoza H. Endothelial cell substrate stiffness influences neutrophil transmigration via myosin light chain kinase-dependent cell contraction. Blood. 2011;118(6):1632.
93. Craig LE, Spelman JP, Strandberg JD, Zink MC. Endothelial Cells from Diverse Tissues Exhibit Differences in Growth and Morphology. Microvascular Research. 1998;55(1):65-76.
94. Rengarajan M, Hayer A, Theriot JA. Endothelial Cells Use a Formin-Dependent Phagocytosis-Like Process to Internalize the Bacterium Listeria monocytogenes. PLoS Pathog. 2016;12(5):e1005603.
95. Greiffenberg L, Sokolovic Z, Schnittler H-J, Spory A, Böckmann R, Goebel W, et al. Listeria monocytogenes-infected human umbilical vein endothelial cells: internalin-independent invasion, intracellular growth, movement, and host cell responses. FEMS Microbiology Letters. 1997;157(1):163-70.
96. Bastounis E, Meili R, Álvarez-González B, Francois J, del Álamo JC, Firtel RA, et al. Both contractile axial and lateral traction force dynamics drive amoeboid cell motility. The Journal of Cell Biology. 2014;204(6):1045-61.

97. Vincent LG, Choi YS, Alonso-Latorre B, del Alamo JC, Engler AJ. Mesenchymal stem cell durotaxis depends on substrate stiffness gradient strength. Biotechnol J. 2013;8(4):472-84.
98. Bastounis E, Meili R, Alonso-Latorre B, del Álamo J, Lasheras J, Firtel R. The SCAR/WAVE complex is necessary for proper regulation of traction stresses during amoeboid motility. Mol Biol Cell. 2011;21(22):3995–4003.
99. Reed SC, Lamason RL, Risca VI, Abernathy E, Welch MD. Rickettsia actin-based motility occurs in distinct phases mediated by different actin nucleators. Curr Biol. 2014;24(1):98-103.
100. Yam PT, Theriot JA. Repeated cycles of rapid actin assembly and disassembly on epithelial cell phagosomes. Mol Biol Cell. 2004;15(12):5647-58.
101. Edelstein AD, Tsuchida MA, Amodaj N, Pinkard H, Vale RD, Stuurman N. Advanced methods of microscope control using μManager software. Journal of Biological Methods; Vol 1, No 2 (2014). 2014.
102. Selinummi J, Seppala J, Yli-Harja O, Puhakka JA. Software for quantification of labeled bacteria from digital microscope images by automated image analysis. Biotechniques. 2005;39(6):859-63.
103. Karhemo P-R, Ravela S, Laakso M, Ritamo I, Tatti O, Mäkinen S, et al. An optimized isolation of biotinylated cell surface proteins reveals novel players in cancer metastasis. Journal of proteomics. 2012;77:87-100.
104. Roesli C, Mumprecht V Fau - Neri D, Neri D Fau - Detmar M, Detmar M. Identification of the surface-accessible, lineage-specific vascular proteome by two-dimensional peptide mapping. (1530-6860 (Electronic)).
105. O'Farrell PH. High resolution two-dimensional electrophoresis of proteins. J Biol Chem. 1975;250(10):4007-21.
106. Burgess-Cassler A, Johansen JJ, Santek DA, Ide JR, Kendrick NC. Computerized quantitative analysis of coomassie-blue-stained serum proteins separated by two-dimensional electrophoresis. Clin Chem. 1989;35(12):2297-304.
107. Oakley BR, Kirsch DR, Morris NR. A simplified ultrasensitive silver stain for detecting proteins in polyacrylamide gels. Anal Biochem. 1980;105(2):361-3.
108. Darie CC, Deinhardt K, Zhang G, Cardasis HS, Chao MV, Neubert TA. Identifying transient protein-protein interactions in EphB2 signaling by blue native PAGE and mass spectrometry. Proteomics. 2011;11(23):4514-28.
109. Shevchenko A, Wilm M, Vorm O, Mann M. Mass spectrometric sequencing of proteins silver-stained polyacrylamide gels. Anal Chem. 1996;68(5):850-8.
110. Sokolowska I, Woods AG, Gawinowicz MA, Roy U, Darie CC. Identification of potential tumor differentiation factor (TDF) receptor from steroid-responsive and steroid-resistant breast cancer cells. J Biol Chem. 2012;287(3):1719-33.
111. Sokolowska I, Dorobantu C, Woods AG, Macovei A, Branza-Nichita N, Darie CC. Proteomic analysis of plasma membranes isolated from undifferentiated and differentiated HepaRG cells. Proteome Sci. 2012;10(1):47.
112. Sokolowska I, Gawinowicz MA, Ngounou Wetie AG, Darie CC. Disulfide proteomics for identification of extracellular or secreted proteins. Electrophoresis. 2012;33(16):2527-36.
113. Spellman DS, Deinhardt K, Darie CC, Chao MV, Neubert TA. Stable isotopic labeling by amino acids in cultured primary neurons: application to brain-derived neurotrophic factor-dependent phosphotyrosine-associated signaling. Mol Cell Proteomics. 2008;7(6):1067-76.

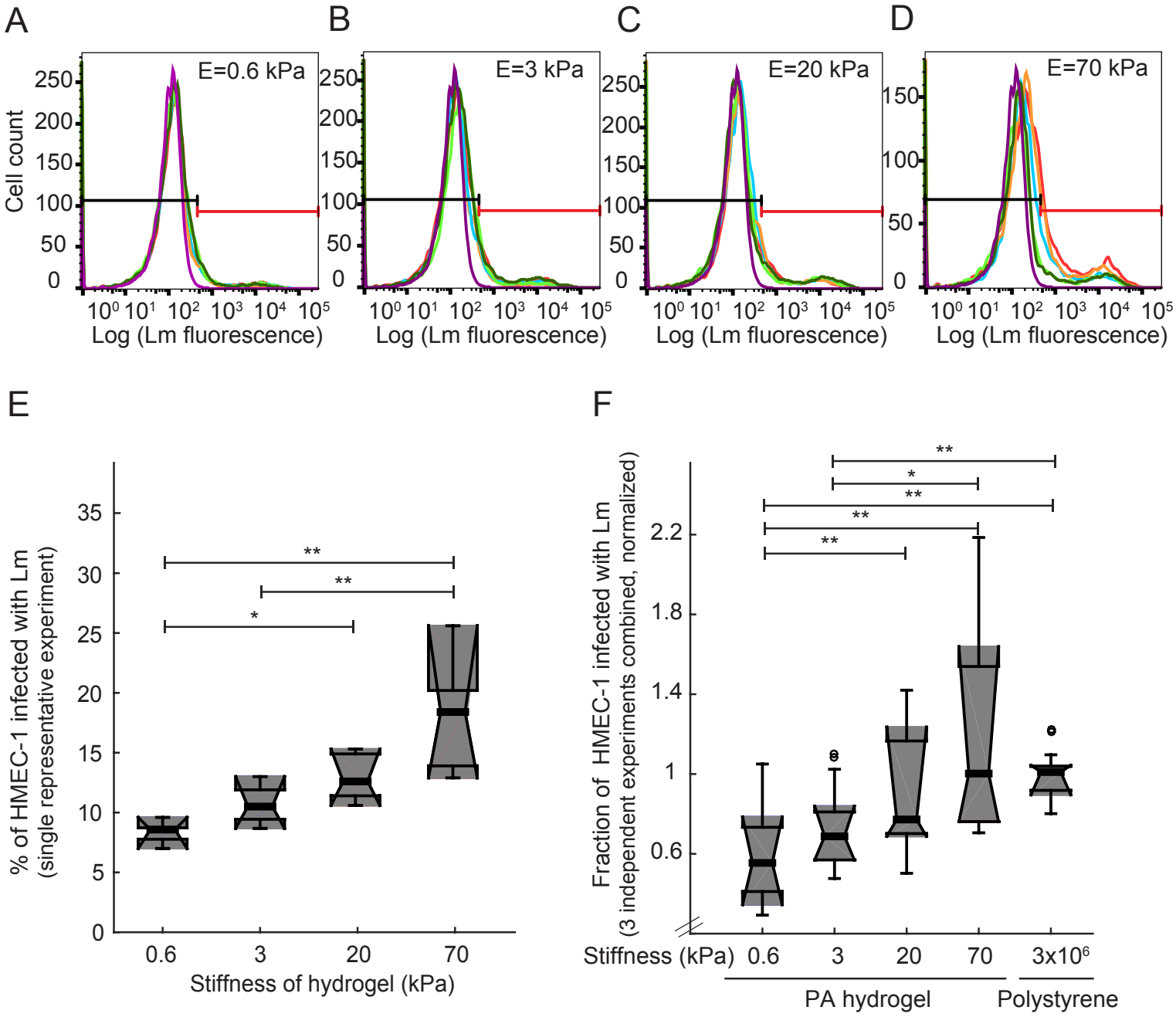
A
B
C
D
E=0.6 kPa
E=3 kPa
E=20 kPa
E=70 kPa
Cell count
Log (Lm fluorescence)
E
F
% of HMEC-1 infected with Lm
(single representative experiment)
Stiffness of hydrogel (kPa)
Fraction of HMEC-1 infected with Lm
(3 independent experiments combined, normalized)
Stiffness (kPa)
PA hydrogel
Polystyrene

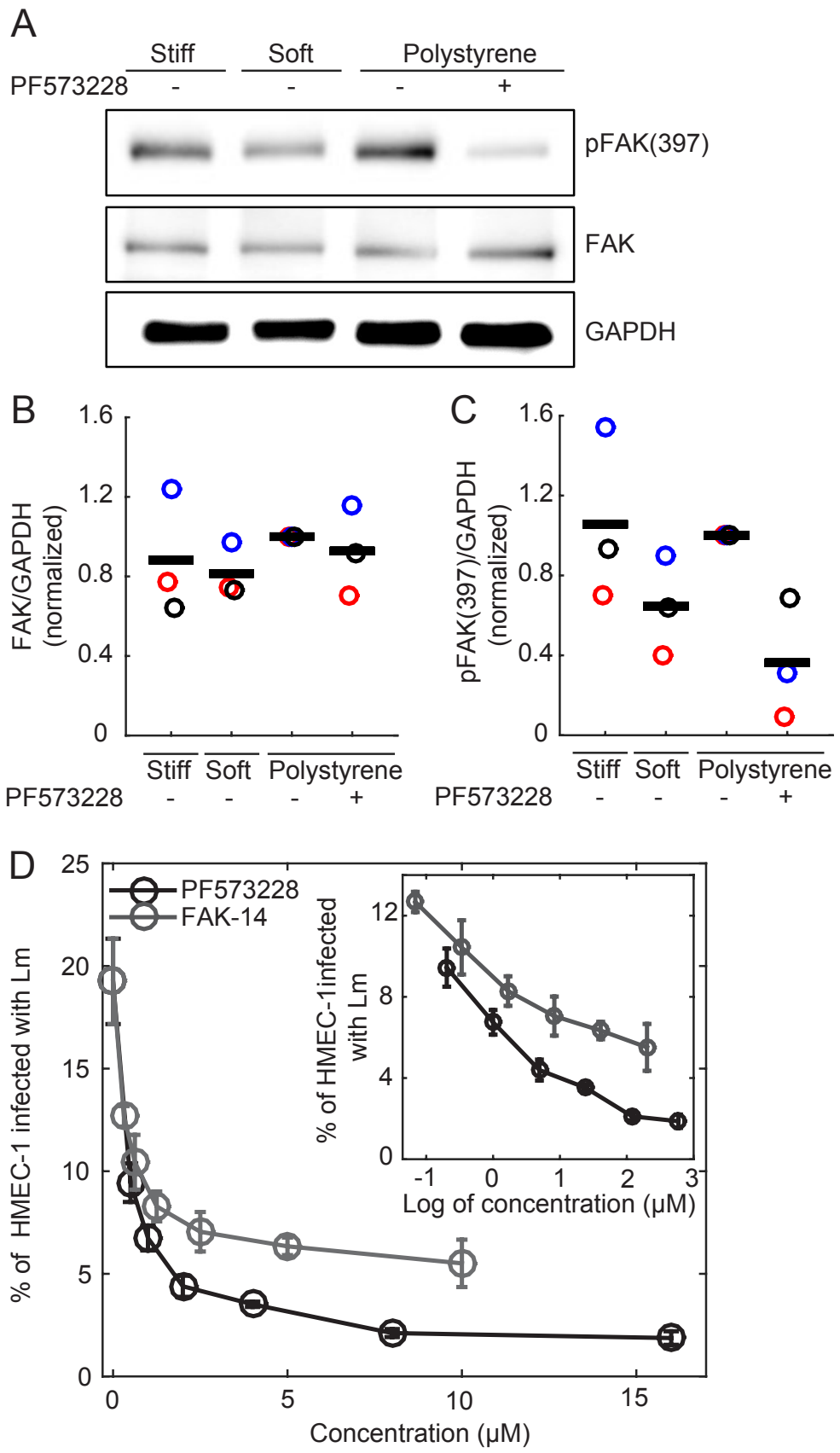
A
Stiff
Soft
Polystyrene
PF573228
-
-
-
+
pFAK(397)
FAK
GAPDH
B
FAK/GAPDH (normalized)
1.6
1.2
0.8
0.4
0
Stiff
Soft
Polystyrene
PF573228
C
pFAK(397)/GAPDH (normalized)
D
PF573228
FAK-14
% of HMEC-1 infected with Lm
Concentration (μM)
Log of concentration (μM)

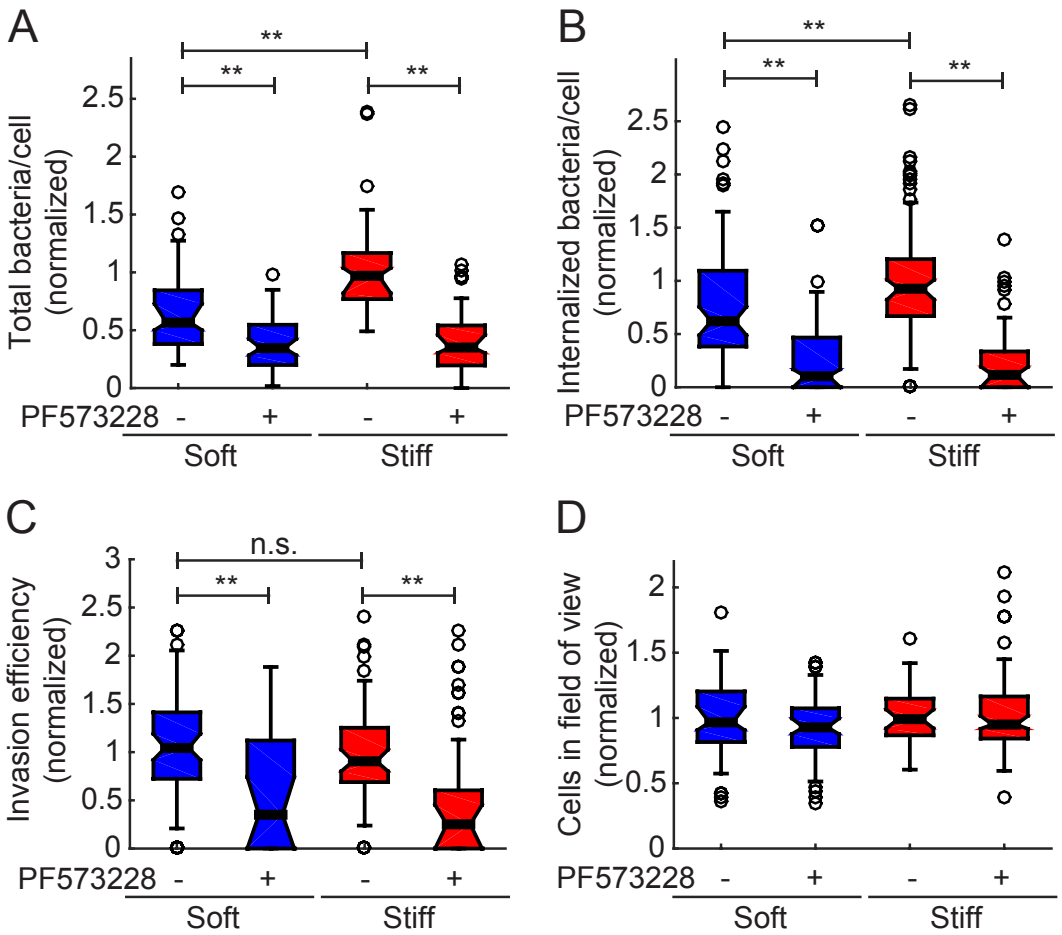
A
Total bacteria/cell (normalized)
**
**
**
PF573228 - + - +
Soft
Stiff
B
Internalized bacteria/cell (normalized)
**
**
**
PF573228 - + - +
Soft
Stiff
C
Invasion efficiency (normalized)
n.s.
**
**
PF573228 - + - +
Soft
Stiff
D
Cells in field of view (normalized)
PF573228 - + - +
Soft
Stiff

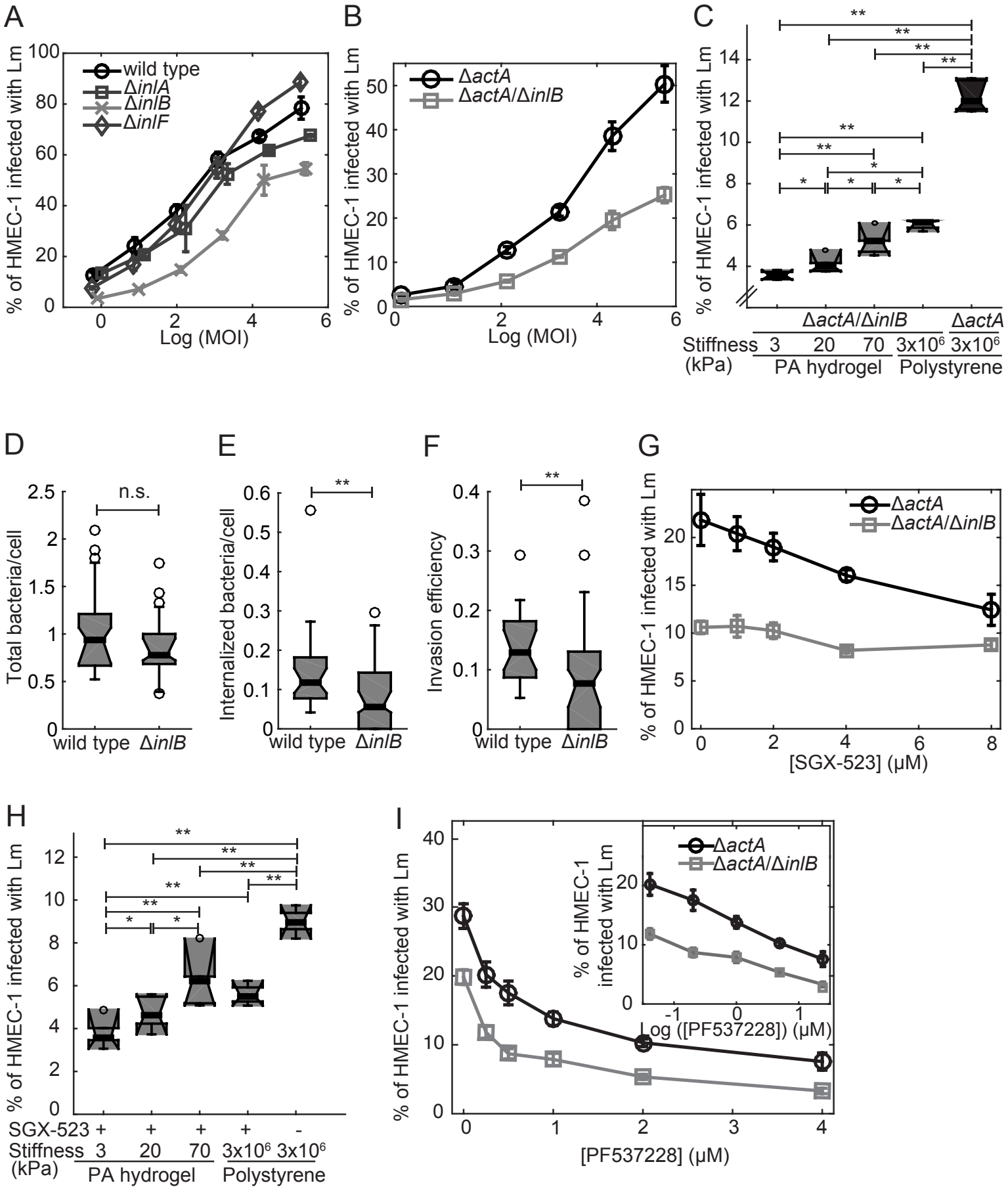
A
% of HMEC-1 infected with Lm
Log (MOI)
wild type
ΔinlA
ΔinlB
ΔinlF
B
% of HMEC-1 infected with Lm
Log (MOI)
ΔactA
ΔactA/ΔinlB
C
% of HMEC-1 infected with Lm
ΔactA/ΔinlB
ΔactA
Stiffness (kPa)
3
20
70
3x10^6
3x10^6
PA hydrogel
Polystyrene
D
Total bacteria/cell
n.s.
wild type
ΔinlB
E
Internalized bacteria/cell
wild type
ΔinlB
F
Invasion efficiency
wild type
ΔinlB
G
% of HMEC-1 infected with Lm
ΔactA
ΔactA/ΔinlB
[SGX-523] (μM)
H
% of HMEC-1 infected with Lm
SGX-523
Stiffness (kPa)
3
20
70
3x10^6
3x10^6
PA hydrogel
Polystyrene
I
% of HMEC-1 infected with Lm
ΔactA
ΔactA/ΔinlB
[PF537228] (μM)
Log ([PF537228]) (μM)

A

HMEC-1 on polystyrene, vehicle control

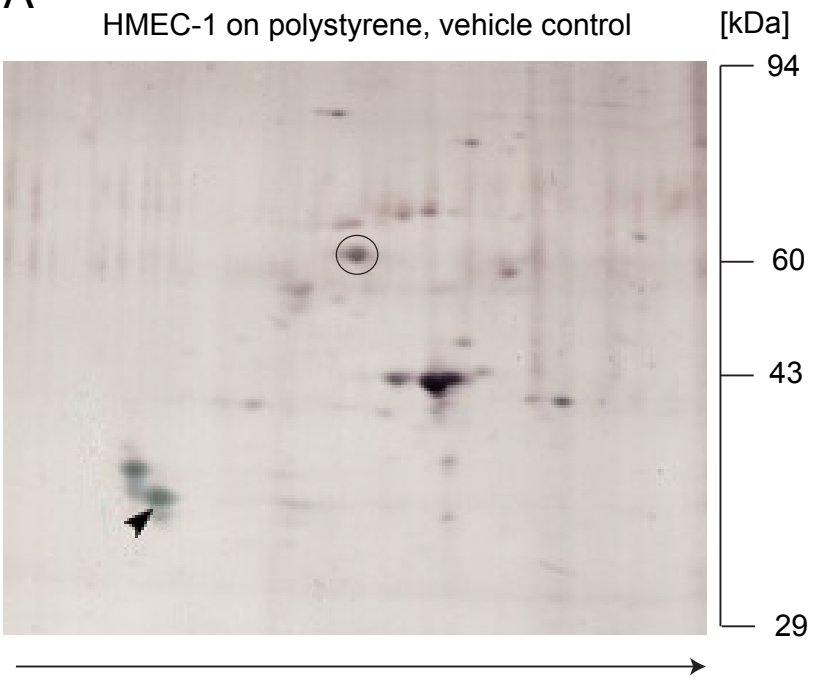

B

HMEC-1 on polystyrene, PF573228

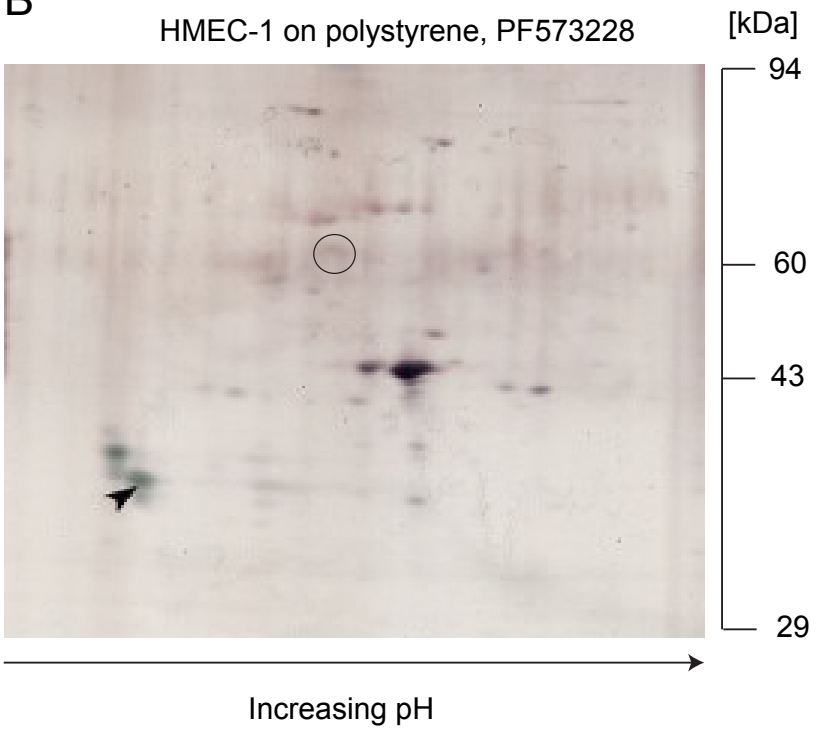

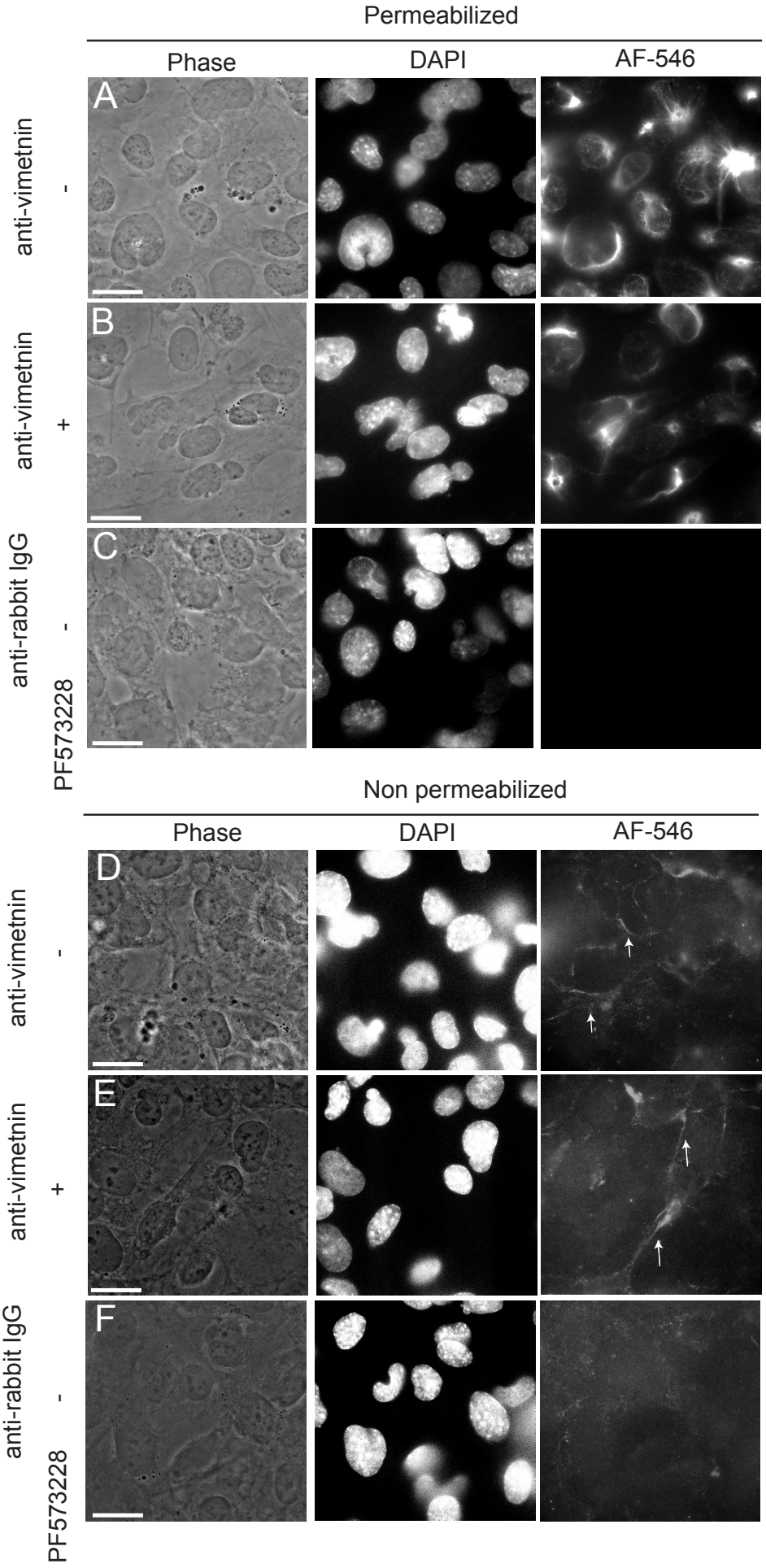
Permeabilized
Phase
DAPI
AF-546
A
B
C
anti-vimetnin
-
anti-vimetnin
+
anti-rabbit IgG
-
PF573228
Non permeabilized
Phase
DAPI
AF-546
D
E
F
anti-vimetnin
-
anti-vimetnin
+
anti-rabbit IgG
-
PF573228

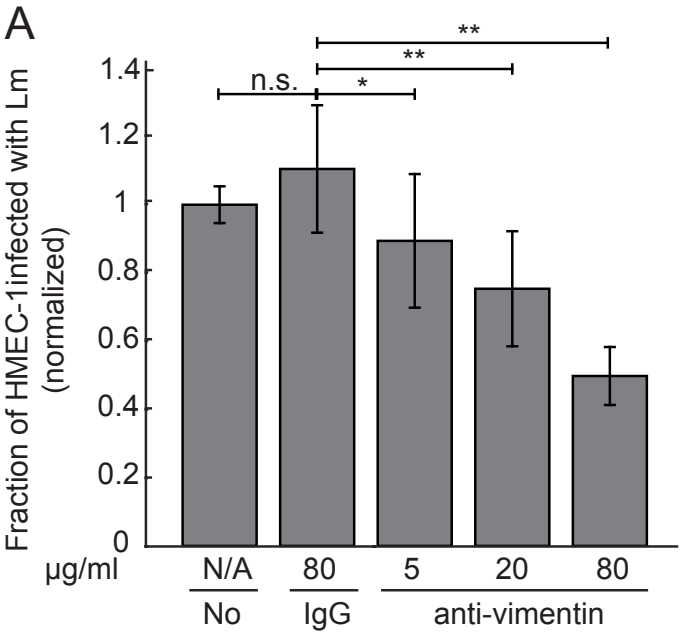
A
Fraction of HMEC-1infected with Lm (normalized)
1.4
1.2
1
0.8
0.6
0.4
0.2
0
n.s.
*
**
**
μg/ml
N/A
80
5
20
80
No
IgG
anti-vimentin

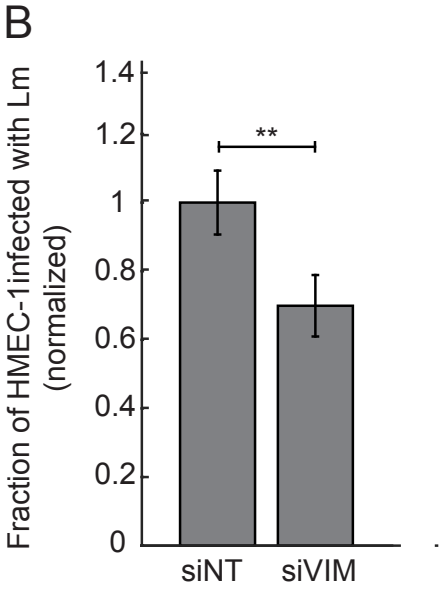
B
Fraction of HMEC-1infected with Lm (normalized)
1.4
1.2
1
0.8
0.6
0.4
0.2
0
**
siNT
siVIM

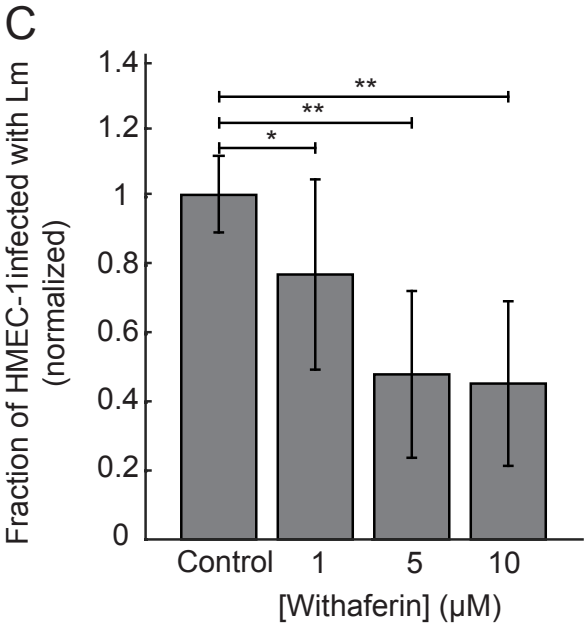
C
Fraction of HMEC-1infected with Lm (normalized)
1.4
1.2
1
0.8
0.6
0.4
0.2
0
*
**
**
Control
1
5
10
[Withaferin] (μM)

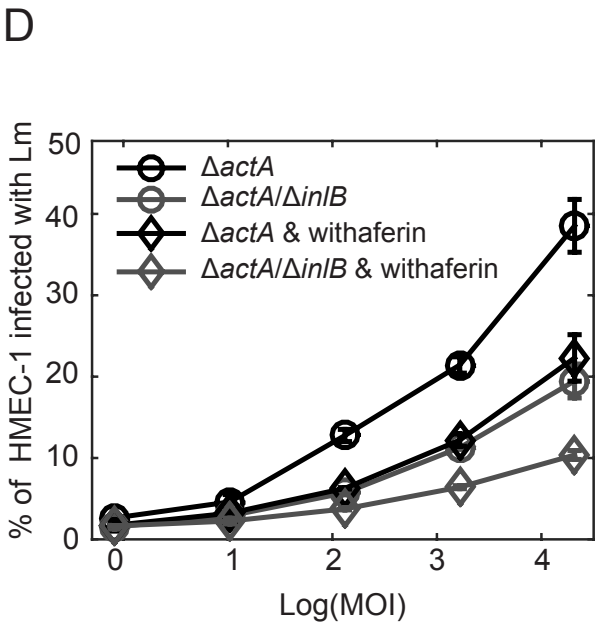
D
% of HMEC-1 infected with Lm
50
40
30
20
10
0
ΔactA
ΔactA/ΔinlB
ΔactA & withaferin
ΔactA/ΔinlB & withaferin
0
1
2
3
4
Log(MOI)

A

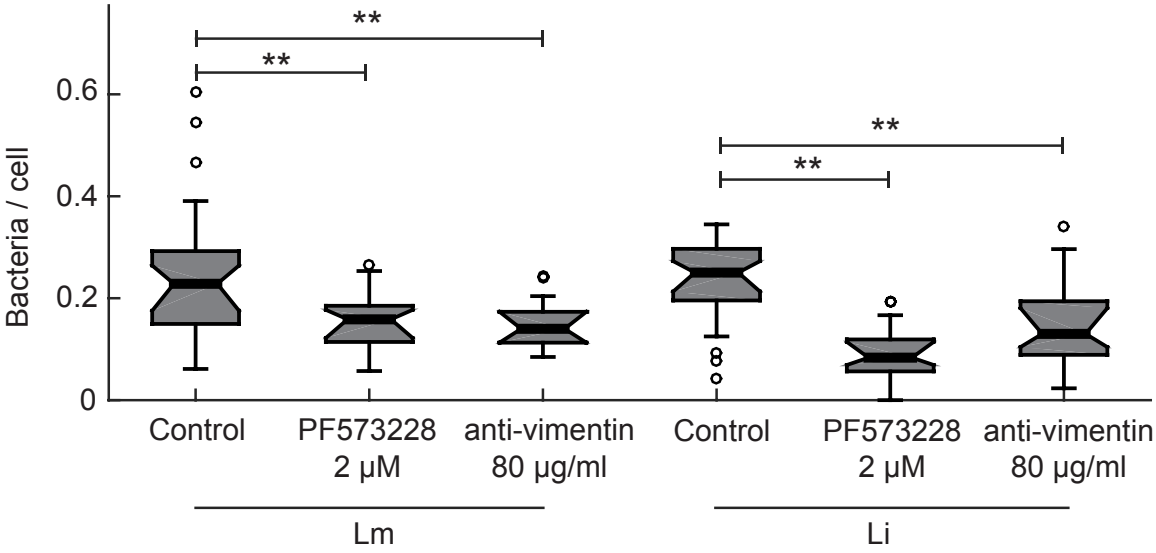
**
**
**
**
Bacteria / cell
0.6
0.4
0.2
0
Control
PF573228
2 μM
anti-vimentin
80 μg/ml
Control
PF573228
2 μM
anti-vimentin
80 μg/ml
Lm
Li

B

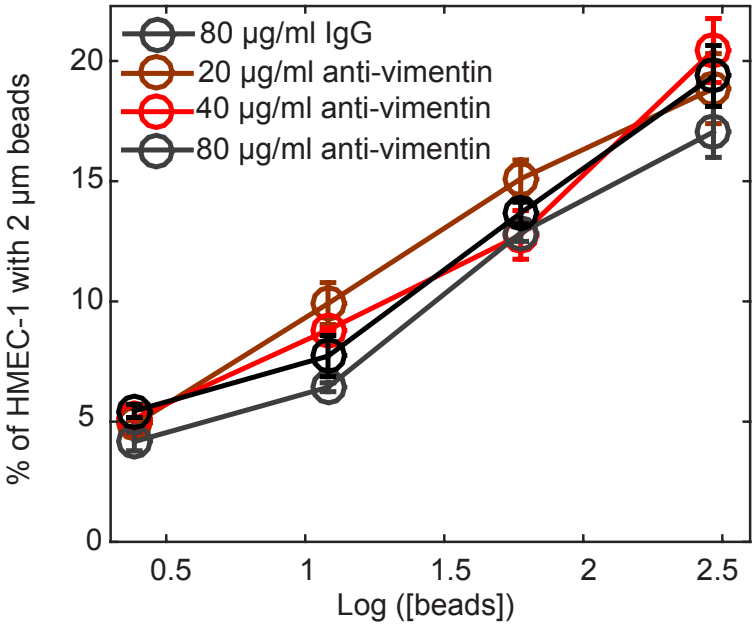
80 μg/ml IgG
20 μg/ml anti-vimentin
40 μg/ml anti-vimentin
80 μg/ml anti-vimentin
% of HMEC-1 with 2 μm beads
20
15
10
5
0
0.5
1
1.5
2
2.5
Log ([beads])

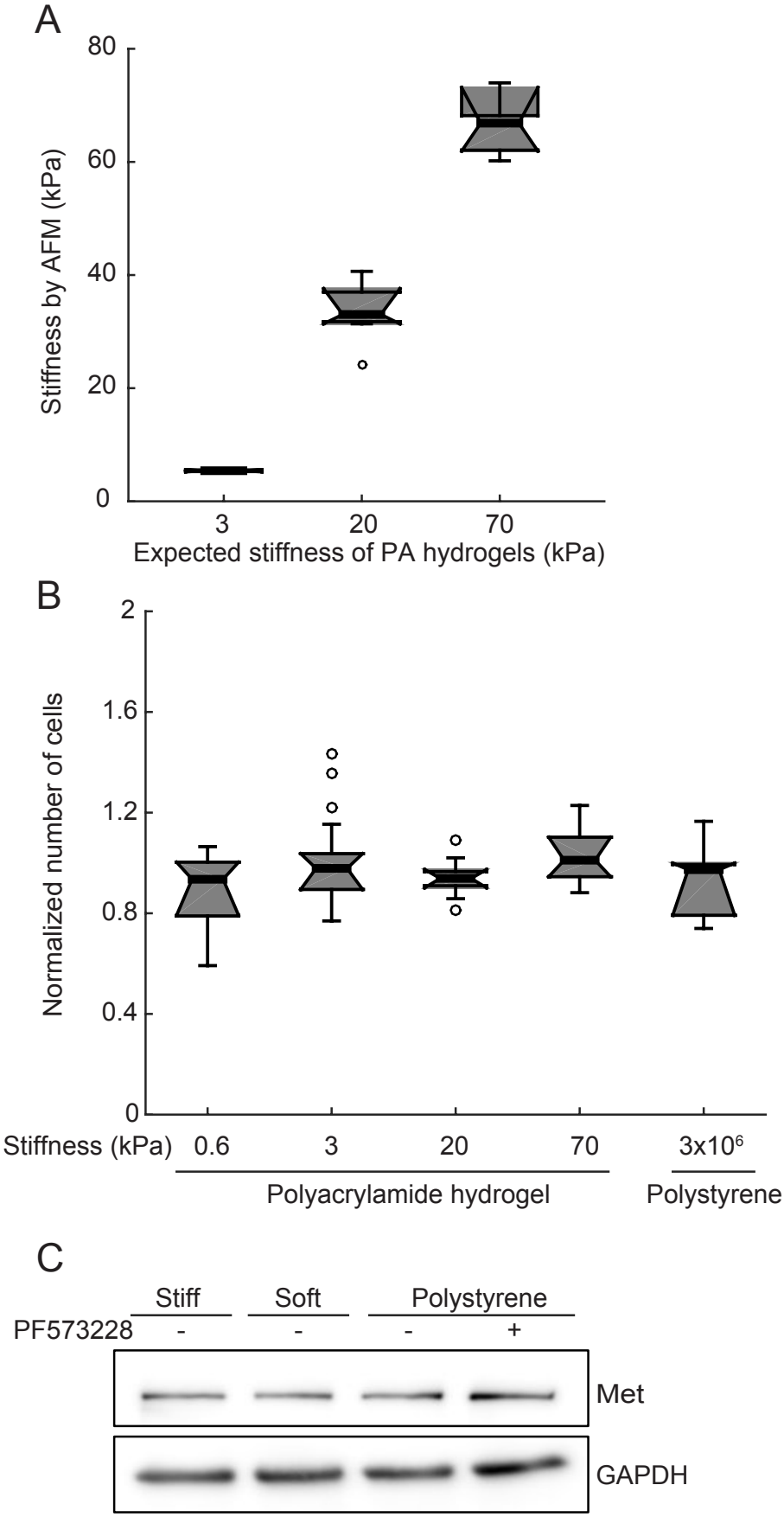
A
80
60
40
20
0
Stiffness by AFM (kPa)
3
20
70
Expected stiffness of PA hydrogels (kPa)
B
2
1.6
1.2
0.8
0.4
0
Normalized number of cells
Stiffness (kPa)
0.6
3
20
70
3x10⁶
Polyacrylamide hydrogel
Polystyrene
C
Stiff
Soft
Polystyrene
PF573228
-
-
-
+
Met
GAPDH

A

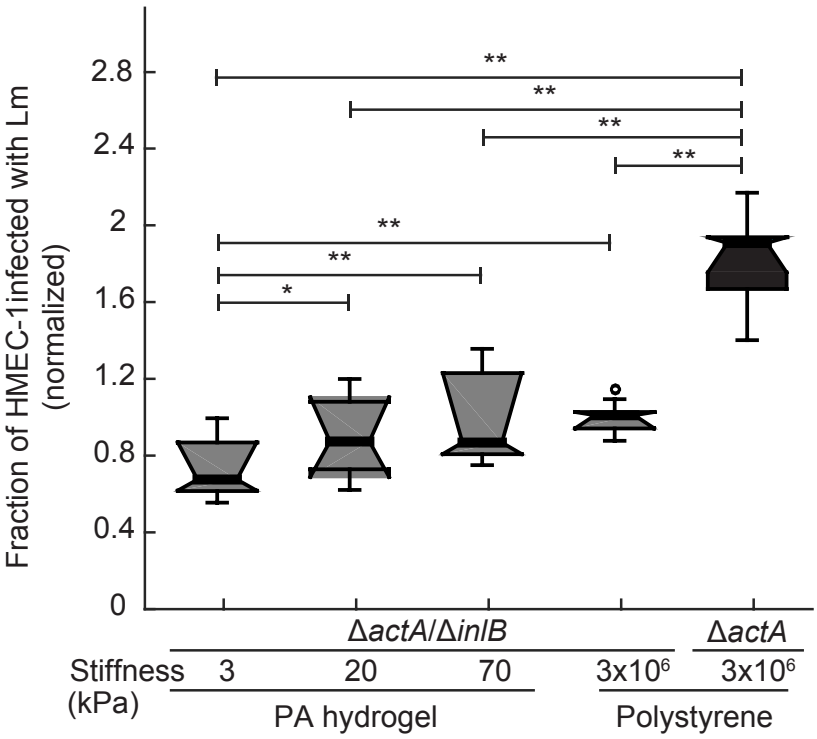
Fraction of HMEC-1infected with Lm (normalized)
2.8
2.4
2
1.6
1.2
0.8
0.4
0
**
**
**
**
**
**
*
ΔactA/ΔinlB
ΔactA
Stiffness (kPa)
3
20
70
3x10^6
3x10^6
PA hydrogel
Polystyrene

B

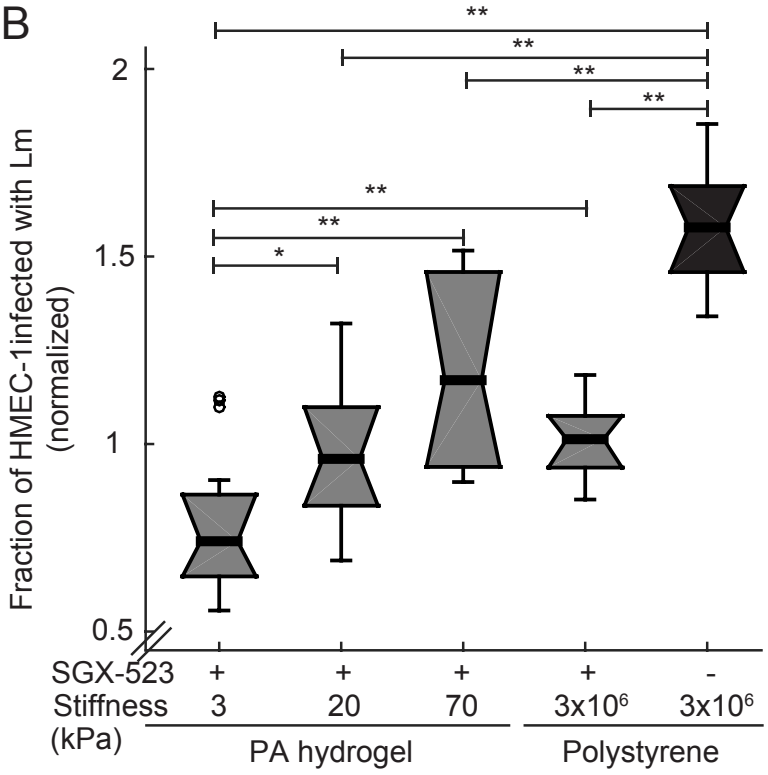
Fraction of HMEC-1infected with Lm (normalized)
2
1.5
1
0.5
**
**
**
**
**
**
*
SGX-523
+
+
+
+
-
Stiffness (kPa)
3
20
70
3x10^6
3x10^6
PA hydrogel
Polystyrene

A

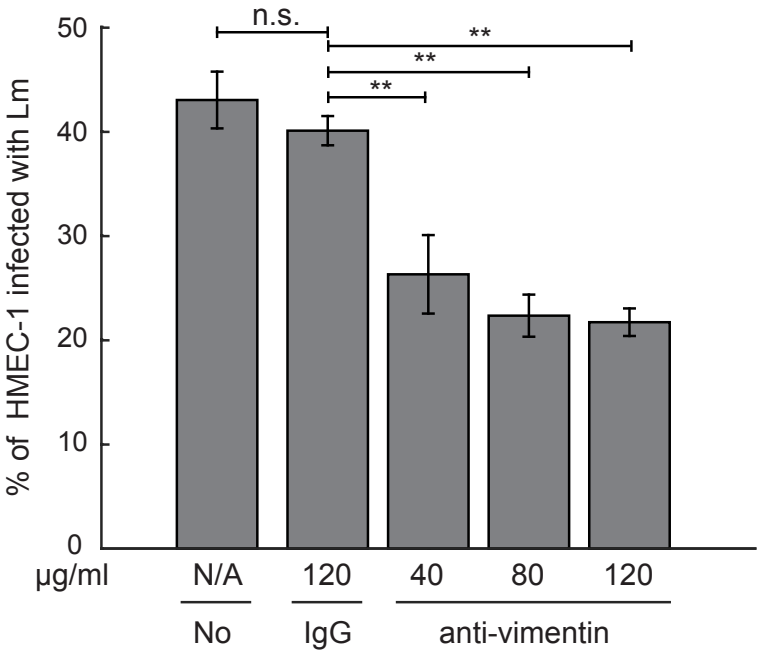
n.s.
**
**
**
% of HMEC-1 infected with Lm
50
40
30
20
10
0
μg/ml
N/A
120
40
80
120
No
IgG
anti-vimentin

B

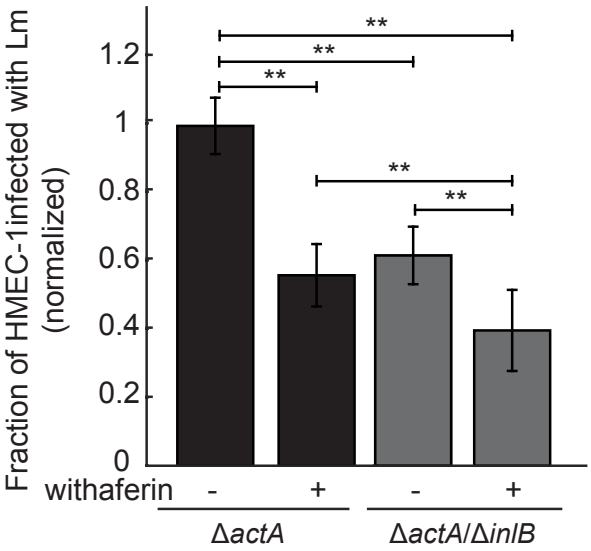
**
**
**
**
**
Fraction of HMEC-1infected with Lm
(normalized)
1.2
1
0.8
0.6
0.4
0.2
0
withaferin
-
+
-
+
ΔactA
ΔactA/ΔinlB

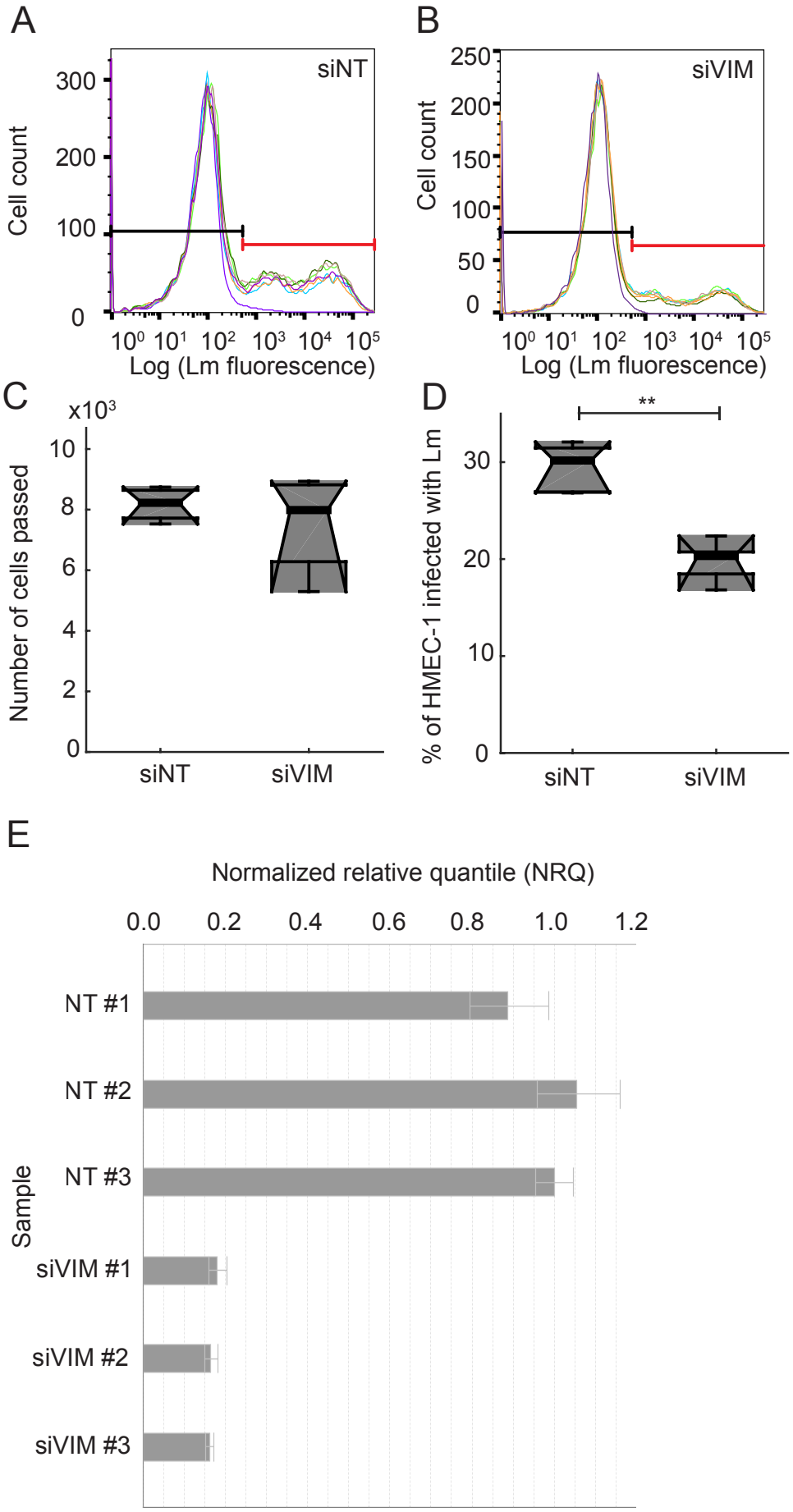
A
siNT
Cell count
300
200
100
0
10^0 10^1 10^2 10^3 10^4 10^5
Log (Lm fluorescence)
B
siVIM
Cell count
250
200
150
100
50
0
10^0 10^1 10^2 10^3 10^4 10^5
Log (Lm fluorescence)
C
x10^3
Number of cells passed
10
8
6
4
2
0
siNT
siVIM
D
**
% of HMEC-1 infected with Lm
30
20
10
0
siNT
siVIM
E
Normalized relative quantile (NRQ)
0.0
0.2
0.4
0.6
0.8
1.0
1.2
Sample
NT #1
NT #2
NT #3
siVIM #1
siVIM #2
siVIM #3